International Communications in Heat and Mass Transfer

https://www.journals.elsevier.com/international-communications-in-heat-and-mass-transfer

Impact factor = 5.683

Accepted November 12th 2021

NUMERICAL STUDY OF TIME-DEPENDENT FLOW OF IMMISCIBLE SAFFMAN DUSTY (FLUID-PARTICLE SUSPENSION) AND ERINGEN MICROPOLAR FLUIDS IN A DUCT WITH A MODIFIED CUBIC B-SPLINE DIFFERENTIAL QUADRATURE METHOD

Rajesh Kumar Chandrawat [A], Varun Joshi[A] and O. Anwar Bég[B]

[A]Department of Mathematics, LP University Jalandhar, ***India.***

[B] Professor and Director-Multiphysical Engineering Sciences Group (MPESG), Dept. Mechanical/Aeronautical Engineering, School of Science, Engineering, Environment (SEE), Salford University, Manchester, M54WT, ***UK.***
Emails: rajesh.16786@lpu.co.in. varunjoshi20@yahoo.com. O.A.Beg@salford.ac.uk

Abstract- Immiscible flows arise in many diverse applications in mechanical, chemical, and environmental engineering. Such flows involve interfacial conditions and often feature mass (species) diffusion. Motivated by applications in non-Newtonian duct processing, in the present article a comprehensive mathematical model and computational simulation with the modified cubic B-spine-Differential Quadrature method (**MCB-DQM**) is described for the unsteady flow of two immiscible fluids - dusty (fluid-particle suspension) and Eringen micropolar fluids - through horizontal channels. Mass transfer is invoked due to particle concentration effects in the dusty fluid. The stable liquid-liquid interface is considered between two immiscible fluids. Fluids are considered to flow under *three different pressure gradients- constant, decaying, and periodic pressure gradient* and the flow characteristics are scrutinized for each case. The coupled partial differential equations are solved with the **MCB-DQM** under physically realistic boundary conditions. Linear velocity, micro-rotation (Eringen angular velocity) is visualized graphically for the effects of the key hydrodynamic and solutal parameters i. e. Reynolds number, particle concentration parameter, Eringen micropolar material parameter, volume fraction parameter, pressure gradient, time, viscosity ratio, and density ratio. The simulations extend the current understanding of two-fluid interfacial duct hydrodynamics and mass transfer and are relevant to chemical engineering separation processing systems.

Keywords: *Dusty fluids, micropolar fluid, immiscible flow, unsteady, interface tracking, volume-of-fluid method, modified cubic B-spline, differential quadrature method, non-Newtonian duct systems.*

Nomenclature

$\emptyset$	The particle volume fraction	ρ_1, ρ_2	The density of lower and upper region fluids
u	The velocity of the fluid.	μ_1, μ_2	viscosity co-efficient lower and upper region fluids
u_p	Particle phase velocity	u_1	the velocity of lower region micropolar fluid
M_*	Microrotations of lower region micropolar fluid	u_2	the velocity of upper region dusty fluid
ρ	The density of the fluid	R	Particle concentration parameter
ρ_p	Particle density	r_1	Ratio of viscosities
μ	Viscosity of fluid	r_2	Ratio of densities
f	The body force	r_3	Particle and fluid density ratio
ξ	The body couple per unit mass	Re	Reynolds number
ω_1, ω_2 and ω_3	gyro-viscosity coefficients	n_1	The micropolar parameter
τ	Gyration parameter	K^*	The stokes drag coefficient

γ_1, ι	Vortex viscosity coefficients	r	The radius of the dust particle
E	The volume transfer coefficient	m_p	The average mass of particles kg

1. Introduction

In many industrial problems, including separation of complex petrochemical liquids, petroleum filtration, polymer technology, slurry dynamics, it is challenging to isolate pure liquids. Often industrial fluent media contain impurities such as dust particles and other suspended contaminants and such fluids are known as “dusty” or “fluid-particle suspensions” and require multi-phase models for their accurate simulation. Thus, in functional applications such as petroleum production, crude oil purification, biochemical separation techniques, etc, the study of two-phase flows is significant where solid spherical objects are distributed in a sterile fluid. Many excellent investigations of the transport phenomena associated with the passage of dusty fluids through conduits (ducts, pipes, channels, etc) have been reported, largely motivated by a desire to explain the fundamental aspects of dust particle and fluid phase interaction in petroleum, biochemical, nuclear, geothermal and also aerospace (fuel) systems. In his pioneering work, Saffman [1] proposed a dusty fluid dynamics framework taking into consideration the impact of suspended particles on laminar flow stability, assuming a homogenous distribution of identical particles in a dusty gas. Michael and Miller[2] derived analytical solutions for a moving dusty gas, which is dispersed uniformly over a rigid plane, considering phase change and oscillatory wave decay as functions of the mass concentration of the dust and that the dusty density greatly exceeds the gas density. Later Peddieson [3] examined boundary-layer characteristics of a quintet of unsteady parallel flows of particulate (dusty) suspensions using the Marble dusty gas model. Mitra and Bhattacharyya [3]–[5]discussed the unstable gas flow between two parallel plates, for a variety of boundary conditions (oscillatory and stationary walls) and in magnetic fields. Chamkha [6] used a finite difference algorithm to compute solutions for dusty heat transfer in a porous walled channel with heat transfer. Attia *et al*. [7]–[9] explored the dusty fluid flow, hydromagnetic dusty Couette flow with heat transfer, and dusty flows in porous media under transpiration wall effects using analytical methods. Attia [10] further investigated the movement of dust particles in non-Newtonian Darcy flow under a magnetic field. Singh *et al.* [11] examined the unstable flow between two oscillating walls in a hydromagnetic channel for viscous, dusty fluid.

Although several studies described earlier have considered non-Newtonian fluid characteristics (viscoelastic, viscoplastic, etc), they have neglected microstructural effects. In real industrial and geophysical systems, suspended particles may spin independently of the suspension fluid medium. This rotation at the microscopic level cannot be simulated with conventional rheological models. Particles in atmospheric flows also exhibit such behavior. The diversion from the direct relationship between pressure and tension of a liquid also contributes to non-Newtonian liquid characteristics. To simulate more precisely the influence of microstructural characteristics on global hydrodynamic behavior, a more complex framework is required. The micropolar theory offers such a framework by extending the conventional linear momentum conservation to include angular momentum conservation of the microelements (“micro-rotation”) in complex fluent media. Physically micropolar fluids represent fluids consisting of rigid, randomly oriented (or spherical) particles suspended in a viscous medium, where the deformation of fluid particles is ignored. The micropolar theory, therefore, features gyratory motions of microelements via the inclusion of an appropriate micro-rotation vector field which permits analysis of different rotational degrees of freedom. Animal, blood, polyurethane solution, liquids with admixtures, rheological slurries, synovial fluid, crude oil, and multiphase geothermal liquids are just some examples of complex media which can be simulated via micropolar fluid dynamics. Eringen [12] introduced micropolar fluid dynamics

in his monumental paper as a special case of his more general micromorphic ("simple microfluid") theory in the mid-1960s. A remarkable aspect of the Eringen formulation is the elegance by which simpler models e. g. Newtonian can be extracted as special cases. The microstructure is simulated with the microrotation vector, extraneous to the *vorticity vector* that creates unsymmetric stress. The theory is also more comprehensive than the Stokes polar (couple stress) model since it includes separate balance equations for micro-rotation providing a more comprehensive picture of microstructural behavior. Micropolar fluid mechanics has been embraced extensively in the engineering and scientific community and has been deployed successfully to investigate an astonishing range of applications spanning hemodynamics, grease tribology, bearing design, orthopedics, drug delivery (pharmacodynamics), sediment transport in river hydraulics, nuclear reactor flows, seeded magnetohydrodynamic energy generator fluid dynamics, ocular biomechanics, vestibular flows, geothermic, biomagnetic peristatic flows, etc. The application of micropolar fluid dynamics for simulation and predicting the flows behavior in microchannels, primarily on the flow field's topology was provided by Kucaba-Pięta1 [13].

Many of these areas have been reviewed by Bég [14]. One of the earliest studies of micropolar *boundary layer flows* was communicated by Peddieson [15] who considered plane or axisymmetric stagnation-point flow of a micropolar fluid over a flat plate and also turbulent shear flows, thereby providing a solid base for future modifications to multi-physics. Apparao *et al*. [16] studied orthopedic lubrication performance with micropolar theory, confirming the superior load-carrying characteristics achieved relative to conventional Newtonian viscous liquids. The microstructural influence on blood rheology characteristics was reported by Kang and Eringen [17]. Devakar and Iyerger [18] investigated the dynamics of micropolar liquids in channels. Jangili *et al.* [19]used a homotopy method to compute the entropy generate rate in hydromagnetic micropolar buoyancy-driven flow in solar ducts. Wang *et al*.[20], [21] examined the motion of micropolar fluids into a micro-parallel system. Gajella *et al.* [22] investigated the thermodynamic optimization of hydromagnetic micropolar Taylor-Couette flow with heat source effects. Further studies of micropolar duct fluid dynamics include Bég *et al*. [23](on non-isothermal Hall hydromagnetic channel flow), Shamshuddin *et al.* [24] (on reactive oscillating micropolar thermo-solutal channel flow) and Bég *et al.* [25](on ion-slip micropolar gas dynamics in a rectangular duct).

There are many applications in engineering sciences and geophysics in which multiple fluids arise which do not mix. These immiscible fluids feature in oil slicks, river contamination, crystal growth, sedimentary reservoir systems, desalination processes, liquid metal fabrication, multi-phase oil pipeline transport, ice accretion on aircraft wings, biopolymeric interfaces, etc. The analysis of immiscible fluid flows has therefore stimulated significant interest in applied mathematics and engineering computation, in parallel with experimental studies. Sherief *et al.*[26] considered the minor deformed interface between two immiscible liquids where one of the fluids is micropolar in the channel and then the Stokes flow generated by a spherical shape particle migrating orthogonal to a planar interface separating two semi-infinite immiscible fluid regimes. They adopted an analytical and numerical technique based on collocation approximation. An excellent appraisal of the viscous Newtonian flow of two immiscible fluids in channel flow has been documented in the classical treatise by Bird *et al*[27]. Some extensive studies of immiscible fluid duct (channel) flows are found in [28]–[31] Umavathi *et al.* [32] provided an analytical solution for the free convective flow of two immiscible fluids (Stokes' polar and viscous Newtonian) in a composite porous medium vertical channel for fully developed laminar conditions. Kumar *et al.* [33] later extended the analysis to micropolar and Newtonian liquids. Srinivas and Ramana Murthy [34] studied the dynamics of

two homogeneous, permeable beds saturated with different density immiscible couple stress (polar) fluids with carefully constructed interfacial boundary conditions. Srinivas *et al.* [35] extended the hydrodynamic model to consider heat transfer effects with entropy generation minimization for a horizontal channel. Srinivas and Ramana Murthy [36] further generalized the studies in a wider range of thermal boundary conditions. Borrelli *et al.* [37] considered two immiscible Newtonian fluids in a vertical channel under a transverse magnetic field, examining buoyancy effects in detail and computing reversed flow phenomena. Ramana Murthy *et al.* [38]extended the studies above for couple stress flows in ducts to consider non-linear thermal radiative effects with an algebraic flux model and homotopy method. Chandrawat *et.al.*[39] explored the flow of two immiscible dusty and non-dusty fluids in the horizontal channel with different geometries.

Most of the studies mentioned above neglected *time effects* i. e. were confined to steady-state analysis. However numerous interfacial duct flows feature transient effects. Time inclusion in mathematical models can provide a deeper insight into the transport phenomena and modifications in flow characteristics can be addressed more accurately. Despite significant relevance to modern industry, relatively little work has however been conducted regarding the time-dependent unstable flow of two immiscible liquids. The unsteady multiphase flow problem has been rigorously explored via the front tracking method by Tryggvason *et al.*[40]. Riaz *et al*. [41] studied the instability of immiscible two-phase flow in porous media. The unstable hydromagnetic flow of immiscible liquids was numerically studied by Vajravelu *et al.*[42] with different permeability of two permeable beds. The unstable oscillatory flow problem with heat transfer of two viscous immiscible fluids through a horizontal channel is studied by Umavathi *et al.*[43]. A study of the coupling effect of heat and mass convection in time-dependent incompressible immiscible viscous fluid flow was presented by Umavathi *et al*.[44].

The extensive spectrum of industrial linear and nonlinear fluid flow problems can be numerically resolved using finite difference, finite element, and finite volume techniques. Devakar and Raje [45] numerically explored the time-dependent unsteady flow of two immiscible fluids with an explicit Crank-Nicolson finite difference method. The low-order approaches do use several grid points to achieve an acceptable degree of accuracy to obtain specific outcomes at such defined points. The differential quadrature method (DQM) was originally proposed by the celebrated Princeton applied mathematician, Richard Bellman [46] in search of an efficient discretization strategy to achieve concise numerical solutions with significantly reduced grid steps. DQM was further improved by Quan and Chang [47], [48]. This technique is also convenient to use and computationally efficient with reduced data complexity, leading to error mitigation and easy implementation. Using the DQM, Katta and Joshi [49] analyzed the behavior of incomprehensible viscoelastic magnetohydrodynamic flow in a porous medium channel. Katta *et al*. [50]again numerically explored the unsteady fluid flow of two immiscible fluids by DQM. DQM has been implemented also for numerical solutions of the two immiscible fluids by Chandrawat *et al*.[51] [52]

A close inspection of the scientific literature has shown that, to the best knowledge of the authors, no attempt has been made thus far to study the *unsteady flow of two immiscible (dusty and micro-polar fluids) with a stable interface*. This is the focus of the present article. Separate scheme of stable interface is considered in a horizontal channel. The velocity profiles for both fluids, micro-rotation (angular velocity) profile, and interface tracking under consideration of both schemes flow and various fluid parameters have been obtained numerically by solving the transformed coupled partial differential equations using the modified cubic B-spline differential quadrature method. The present study has significant

applications in a range of technologies including transient two-phase transport in energy generator ducts [53], hemodynamic flow separation[54], [55], and biological pump designs [56].

2. Mathematical model for micropolar-dusty two-fluid immiscible duct flow

The field equations governing the dusty fluid flow are following [7]:

Continuity equation:

$$\emptyset_t - \nabla.((1-\emptyset)u) = 0 \quad (1)$$

$$\emptyset_t - \nabla.(\emptyset u_p) = 0 \quad (2)$$

Fluid and Particulate phase momenta equations:

$$\rho\,(1-\emptyset).\left(\frac{\partial u}{\partial t} + u.\nabla\, u\right) = (1-\emptyset)(-\nabla p + \mu\nabla^2 u) - E\rho_{\,p}\emptyset(u-u_P) \quad (3)$$

$$\rho_{\,p}\emptyset\,\left(\frac{\partial u_P}{\partial t} + u_P.\nabla u_P\right) = E\rho_{\,p}\emptyset\left(u-u_p\right) \quad (4)$$

Micropolar fluid flow field equations are given following Eringen [13]:

$$\rho_{\,t} + \nabla.(\rho\, u) = 0 \quad (5)$$

$$\nabla p - \iota\nabla\times M + \rho\,.\frac{\partial u}{\partial t} = \rho\, f + (\mu+\iota)\nabla\times\nabla\times u + (\gamma_1 + 2\mu + \iota)\nabla(\nabla.u) \quad (6)$$

$$\rho\,.\tau\frac{\partial M}{\partial t} + \iota\nabla\times v = \rho\,\xi - 2\iota M + \omega_1\,\nabla\times\nabla\times M - (\omega_1+\omega_2+\omega_3)\nabla(\nabla.M) \quad (7)$$

Here $\emptyset$ is the particle volume fraction, u is the velocity of the respective dusty and micropolar fluid, u_p is the velocity of a dust particle, M is the micro-rotation vector of micropolar fluid, ρ is the density of the fluid, p is the fluid pressure at any point, $\rho_{\,p}$ is the density of dust particles, the material constants γ_1, ι and μ are viscosity coefficients for respective fluids, f is the body force, ξ is the body couple per unit mass, $\omega_1, \omega_2\ and\ \omega_3$ are gyro-viscosity coefficients, τ Gyration parameter and E is the volume transfer coefficient for dust particles. Some assumptions have been made to develop the governing equations regarding the analysis of dusty fluids (fluid-particle suspensions). The fluid is incompressible, and its density is believed to be stable for both phases. The dust particles are in an electro-free form and circular in shape. All the dust particles have the same size, mass, are non-deformable, and are homogeneously distributed throughout the fluid. If the dusty fluid flows across the channel (duct) boundaries, then particles cannot exit via the walls. It is also assumed that the particle phase is sufficiently dilute such that the interactions between any two particles are ignored, and the dust particle size is also relatively tiny in scale. Hence the *net dust effect on the fluid particles* is equivalent to the additional force$E\rho_{\,p}\emptyset(u-u_p)$ per unit volume.

2.1. Formulation of dusty and Micro-polar fluid flow

Consider the unsteady, fully developed, laminar, unidirectional, immiscible, incompressible viscous flow of Eringen micropolar and Saffman dusty fluids. Some assumptions are invoked under Scheme-I. Both fluids move between two horizontal parallel non-porous plates. Both plates are electrically non-conductive. The plates are located in the *X-Z* plane as depicted in **Figure 1**. Eringen micropolar fluid occupies the lower channel half-space (zone) i. e. zone I ($-k \le y \le 0$) and *possesses* the fluid velocity u_1, density $\rho_{\,1}$, viscosity μ_1. Saffman dusty fluid occupies the upper half-space zone, zone II ($0 \le y \le k$) and possesses fluid velocity u_2, density $\rho_{\,2}$, viscosity μ_2.In the dusty fluid, the dust particles have particle velocity u_p, and density $\rho_{\,p}$. The transportation attributes are unchanged in both the zones and the common pressure

gradients are applied from the horizontal (*X*) axial direction. The flow of dusty fluid in Zone –II is governed by the equations (1),(2),(3), and (4) and the flow of micropolar fluid in Zone –I is governed by the equation (5),(6), and (7). The fluid velocity vectors in both zones (*i=I, II*) are $u_i(y,t)$), particle velocity is $u_p(y,t)$ in zone II (upper), and the micro-rotation vector $M_*(y,t)$ in zone I (lower) are assumed to be (u_i=($u_i(y,t)$,0,0) , (u_p=($u_p(y,t)$,0,0) and ($M = (0,0,M_*(y,t))$ respectively. The movement of fluids is incompressible unsteady and driven by an applied pressure gradient in the *X*-axial direction; therefore, the velocity profile is unidirectional. The fluid layers are mechanically coupled through the mode of momentum exchange. Transferring momentum arises through consistency in velocity and shear stress *over the interface*. However, we assume that the flow rate and shear pressure are also stable at the interface between two liquids. Fluid flow and micro-rotation distribution under the aforesaid assumed constraints take the form:

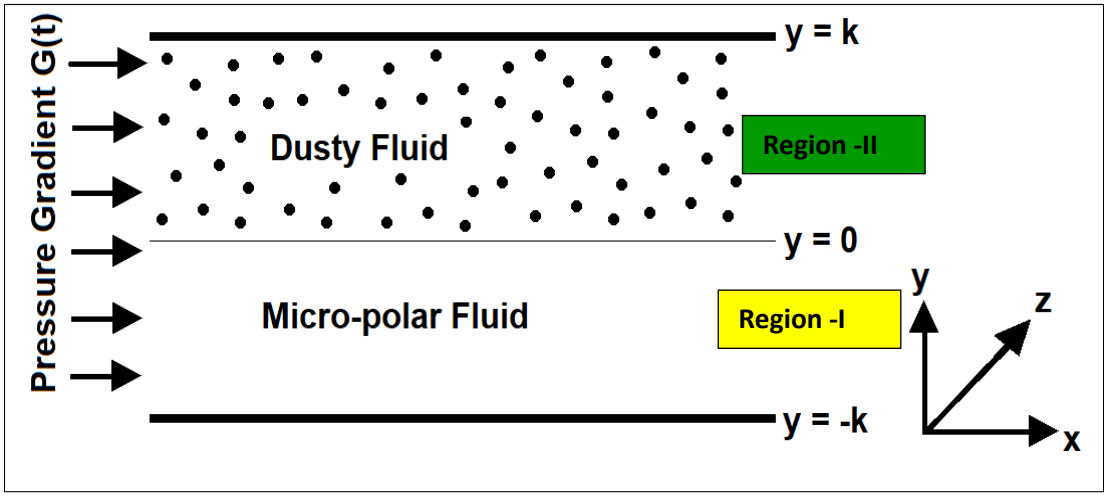

Figure 1: Geometrical configuration of Couette flow of dusty and micropolar fluids under the scheme-I.

Zone-I (Micropolar fluid: −k ≤ y ≤ 0).

$$\nabla.(\rho\, u_1) = 0 \tag{8}$$

$$\rho_1.\frac{\partial u_1}{dt} = -\nabla p + \iota\,\frac{\partial M_*}{\partial y} + (\mu_1 + \iota)\frac{\partial^2 u_1}{\partial y^2} \tag{9}$$

$$\rho_1.\tau\frac{\partial M_*}{\partial t} = -2\iota M_* - \iota\,\frac{\partial u_1}{\partial y} + \omega_1\,\frac{\partial^2 M_*}{\partial y^2} \tag{10}$$

Zone-II (Dusty fluid: 0 ≤ y ≤ k)

$$\rho_2.\frac{\partial u_2}{\partial t} = -\nabla p + \mu_2\frac{\partial^2 u_2}{\partial y^2} - E\rho_p\emptyset\frac{(u_2-u_p)}{(1-\emptyset)} \tag{11}$$

$$\frac{\partial u_p}{\partial t} = E(u_2 - u_p) \tag{12}$$

Classical hyper-stick and no-slip boundary conditions are considered and can be numerical as

Initial conditions: At $t \leq 0$,

$$u_1(y,t) = 0\ for - k \leq y \leq 0 \tag{13}$$

$$M_*(y,t) = 0\ for - k \leq y \leq 0 \tag{14}$$

$$u_2(y,t) = 0\ for\ 0 \leq y \leq k \tag{15}$$

$$u_p(y,t) = 0 \; for \; 0 \le y \le k \tag{16}$$

Boundary and interface conditions: At $t > 0$,

$$u_1(-k,t) = 0 \tag{17}$$

$$u_2(k,t) = 0 \tag{18}$$

$$u_p(k,t) = 0 \tag{19}$$

$$M_*(-k,t) = 0 \tag{20}$$

The fluid velocities and shear stress are both continuous at the liquid-liquid interface [45], [57], [58] These constraints can be expressed mathematically as follows.

$$u_1(0,t) = u_2(0,t) \tag{21}$$

As the microrotation is proportional to the couple stress at the boundary (At the interface), hence the general form of the interfacial condition for angular velocity M_**especially for the droplet case can be considered as adopted in Niefer and Kaloni [59], Faltas and Saad [60]. However, in the current study, we chose the interfacial condition for microrotation(spin–vorticity) [45][57][58] over other existing conditions at *y=0,* because it is realistic and consistent to apply at the interface between two immiscible fluids.

$$M_*(0,t) = -\frac{1}{2}u_{1_y} \tag{22}$$

$$\mu_2 u_{2_y} = (\mu_1 + \iota)u_{1_y} + \iota M_* \quad at \; y = 0 \tag{23}$$

Introducing the non-dimensional parameters $\bar{x} = \frac{x}{k}, \bar{y} = \frac{y}{k}, \overline{u_1} = \frac{u_1}{U_0}, \overline{u_2} = \frac{u_2}{U_0}, \overline{u_p} = \frac{u_p}{U_0}, \; \bar{p} = \frac{p}{\rho_1 {U_0}^2}, \bar{t} = \frac{tU_0}{k}, \quad \lambda_1 = (\mu_1 + \iota/2)\tau$ with $\tau = k^2$ and $n_1 = \frac{\iota}{\mu_1}$ and $E = \frac{6\pi r \mu_2}{m_p}$ is the volume transfer coefficient with an average mass of dust particle m_p and radius r. Hence the last term of equation (11) $E\rho_p \emptyset \frac{(u_2 - u_p)}{(1-\emptyset)}$ can be written as $\frac{R * r_1}{Re * r_2}\left(u_2 - u_p\right)$ where $R = \frac{K^* N k^2 \emptyset}{\mu_2 (1-\emptyset)}$ is particle concentration parameter and $K^* = 6\pi r \mu_2 U_0$ is the Stokes drag coefficient, N is the number density of particle per unit volume, and $Re = \frac{\rho_1 U_0}{\mu_1}$ is the Reynolds number. $r_1 = \frac{\mu_2}{\mu_1}, r_2 = \frac{\rho_2}{\rho_1}$ are the ratio of viscosity and density of the two liquids, respectively. Hence the last term of equation (12) is updated accordingly where $r_3 = \frac{\rho_2}{\rho_p}$ denotes the ratio of density of fluid to the density of dust particles in Zone II. $-\nabla \mathrm{p} = -\partial \mathrm{p}/\partial \mathrm{x} = Ge(t)$ is the applied time dependent pressure gradient in the x-axial direction with $t > 0$ .Three distinct cases for $Ge(t)$ are considered in the numerical analysis:

Case-I: $Ge(t)$ = Ge (If the fluid flow is triggered by an applied *constant* pressure gradient)

Case-II: $Ge(t)$ = $Ge * Sin(wt)$ (If the fluid flow is triggered by an applied *periodic* pressure gradient with oscillating parameter w)

Case-III: $Ge(t)$ = $Ge * e^{-\lambda t}$ (If the fluid flow is triggered by a *decaying* pressure gradient with decaying parameterλ).

After dropping the bars and introducing the above non-dimensional parameters and appropriate initial, interfacial, and boundary conditions, according to the scheme-I, the equations emerge as:

Zone-I ($-k \le y \le 0$) (micropolar liquid zone):

$$u_{1_t} = \frac{Ge(t)}{Re} + \frac{n_1 M_{*y}}{Re} + \frac{(n_1+1)u_{1yy}}{Re} \tag{24}$$

$$M_{*_t} = \frac{(2+n_1)M_{*yy}}{2Re} - \frac{n_1(2M_* + u_{1_y})}{Re} \quad (25)$$

Zone-II (0 ≤ y ≤ k) (Saffman dusty fluid zone):

$$u_{2_t} = \frac{Ge(t)}{r_2} + \frac{r_1}{r_2}\frac{u_{2yy}}{Re} - \frac{R*r_1}{r_2}\frac{(u_2-u_p)}{Re} \quad (26)$$

$$u_{p_t} = \frac{R*r_3*r_1}{r_2}\frac{(u_2-u_p)}{Re} \quad (27)$$

Eqns. *(13)-(23)* are considered as initial, interfacial, and boundary conditions with $k = 1$

3. Numerical solution by differential quadrature method

To analyze micro-rotational and velocity behavior followed by the scheme, we split the domain [-1, 1] for micro-polar liquid (zone-I) in [-1, 0] and dusty fluid in [0, 1] (Zone-II) then both domains are likewise discretized with step length *h* in y-axial directional and k'in the time scales. The nodes are presumed to disperse uniformly.

$U = y_1 < y_2 < \cdots < y < y_n = b$, such that $y_{i+1} - y_i = h$ on the real axis. *(28)*

After that I, and II order derivatives of $u_1(y,t), u_2(y,t), M_*(y,t), u^*(y,t), and\ C_i(y,t)$ are obtained at any time on the *nodes* x_i,

For $= 1,2,3, \dots, n$.

$$u_{1_y}(y_i,t) = \sum_{j=1}^{N} U^*_{ij} u_1(y_j,t), \text{ for } j = 1,2,\dots,N \quad (29)$$

$$u_{1_{yy}}(y_i,t) = \sum_{j=1}^{N} V^*_{ij} u_1(y_j,t), \text{ for } j = 1,2,\dots,N \quad (30)$$

$$u_{2_y}(y_i,t) = \sum_{j=1}^{N} U^*_{ij} u_2(y_j,t), \text{ for } j = 1,2,\dots,N \quad (31)$$

$$u_{2_{yy}}(y_i,t) = \sum_{j=1}^{N} V^*_{ij} u_2(y_j,t), \text{ for } j = 1,2,\dots,N \quad (32)$$

$$M_{*_y}(y_i,t) = \sum_{j=1}^{N} U^*_{ij} M_*(y_j,t), \text{ for } j = 1,2,\dots,N \quad (33)$$

$$M_{*_{yy}}(y_i,t) = \sum_{j=1}^{N} V^*_{ij} M_*(y_j,t), \text{ for } j = 1,2,\dots,N \quad (34)$$

Here U^*_{ij} $V^*_{ij}$are the respective weighting coefficients of first and second-order derivative coefficients concerning *y* measured by MCB-Spline functions. The functions of the knots are mentioned below.

$$\varphi_j(y) = \frac{1}{h^3}\begin{cases} (y-y_{j-2})^3, & y\epsilon\,[y_{j-2}, y_{j-1}) \\ (y-y_{j-2})^3 - 4(y-y_{j-1})^3, & y\epsilon[y_{j-1}, y_j) \\ (y_{j+2}-y)^3 - 4(y_{j+1}-y)^3, & y\epsilon\,[y_j, y_{j+1}) \\ (y_{j+2}-y)^3, & y\epsilon[y_{j+1}, y_{j+2}) \\ 0, & otherwise\ . \end{cases} \quad (35)$$

where $\{\varphi_0(y), \varphi_1(y), \varphi_2(y) \dots, \varphi_{n+1}(y)\}$ are the basis function over the region [a, b]. The basis function is updated as follows to get a system of equations that could be expressed by a diagonal-dominated matrix [50].

$$\left.\begin{array}{c}\psi_1(y)=\varphi_1(y)+2\varphi_0(y)\\ \psi_2(y)=\varphi_2(y)-\varphi_0(y)\\ \psi_j(y)=\varphi_j\,,for\ j=3,\ldots.N-2\\ \psi_{N-1}(y)=\ \varphi_{N-1}(y)-\varphi_{N+1}(y)\\ \psi_N(y)=\varphi_N(y)+2\varphi_{N+1}(y)\end{array}\right\} \quad (36)$$

The derivative of the basic functions are as follows:

$$\varphi_j{}'(y)=\frac{1}{h^3}\begin{cases}3\left(y-y_{j-2}\right)^2, & y\epsilon\,[y_{j-2},y_{j-1})\\ 3\left(y-y_{j-2}\right)^2-12\left(y-y_{j-1}\right)^2, & y\epsilon[y_{j-1},y_j)\\ -3\left(y_{j+2}-y\right)^2+12\left(y_{j+1}-y\right)^2, & y\epsilon\,[y_j,y_{j+1})\\ -3\left(y_{j+2}-y\right)^2, & y\epsilon[y_{j+1},y_{j+2})\\ 0, & otherwise\,.\end{cases} \quad (37)$$

$$\left.\begin{array}{c}\psi'_1(y)=\varphi'_1(y)+2\varphi'_0(y)\\ \psi'_2(y)=\varphi'_2(y)-\varphi'_0(y)\\ \psi'_j(y)=\varphi'_j\,,for\ j=3,\ldots.N-2\\ \psi'_{N-1}(y)=\ \varphi'_{N-1}(y)-\varphi'_{N+1}(y)\\ \psi'_N(y)=\varphi'_N(y)+2\varphi'_{N+1}(y)\end{array}\right\} \quad (38)$$

The estimate of the first-order derivative is

$$\psi'_k(y_i)=\sum_{j=1}^{N}U^*{}_{ij}\varphi_k(y_j) \qquad \begin{array}{l}for\ i=1,2,\ldots,N\\ k=1,2,\ldots,N\end{array} \quad (39)$$

Then using $U^*{}_{ij}\ for\ i=1,2,\ldots,N$ in equation (18) the following tri-diagonal system of equation is established as

$$\begin{bmatrix}6&1&0&0&&&&&\\0&4&1&0&\cdots&0&&0&\\0&1&4&1&&&&&\\&\vdots&&0&\ddots&0&&\vdots&\\&&&&&1&4&1&0\\&0&&0&\cdots&0&1&4&0\\&&&&&0&0&1&6\end{bmatrix}\begin{bmatrix}U^*{}_{i1}\\U^*{}_{i2}\\U^*{}_{i3}\\.\\.\\.\\.\\,\\U^*{}_{iN-1}\\U^*{}_{iN}\end{bmatrix}=\begin{bmatrix}\psi'_1(y_i)\\\psi'_2(y_i)\\\psi'_3(y_i)\\.\\.\\.\\.\\,\\\psi'_{N-1}(y_i)\\\psi'_N(y_i)\end{bmatrix} \quad (40)$$

Solving the above system the weighting coefficients $\{U^*{}_{1,1}\ ,\ U^*{}_{1,2}\ldots,U^*{}_{iN}\}$, $\{U^*{}_{2,1}\ ,\ U^*{}_{2,2}\ldots,U^*{}_{2N}\},\ldots.,\{U^*{}_{N,1}\ ,\ U^*{}_{N,2}\ldots,U^*{}_{NN}\}$, of 1st order derivatives of linear and angular velocities, are obtained, and then the value of $W_{i,j}^{(2)}$ for $i=1,2,3\ldots N, j=1,2,3\ldots N$ is calculated as follows

$$\left.\begin{array}{ll}V^*{}_{ij}=2U^*{}_{ij}\left(U^*{}_{ij}-\frac{1}{y_i-y_j}\right) & \text{for } i\neq j\\ V^*{}_{ii}=-\sum_{i=1,i\neq j}^{N}V^*{}_{ij} & for\ i=j\end{array}\right\} \quad (41)$$

3.1. Computation of velocity and microrotation profiles

To obtain the velocity and micro-rotation profiles for Saffman dusty and Eringen micropolar fluids in the respective Zones under the scheme-I, one may replace the approximation of the spatial components of the I and II order obtained by using

MCB-DQM. Hence the system of coupled partial equations (24)-(27) followed by schemes numerically solved with the initial and boundary conditions (13)-(23) and the linear velocities and angular velocity component (microrotation) profiles of both fluids and particles are readily obtained. The equations (24)-(27) can be updated as follows:

Zone-I ($-k \le y \le 0$) (micropolar liquid zone):

$$u_{1_t}=Ge(t)+\frac{n_1}{Re}\left(\sum_{j=1}^{N} U^*{}_{ij} M_*(y_j,t)\right)+\frac{(n_1+1)}{Re}\left(\sum_{j=1}^{N} V^*{}_{ij} u_1(y_j,t)\right) \quad (42)$$

$$M_{*t}=\frac{(n_1+2)}{2Re}\left(\sum_{j=1}^{N} V^*{}_{ij} M_*(y_j,t)\right)-\frac{n_1}{Re}\left(2M_*+\sum_{j=1}^{N} U^*{}_{ij} u_1(y_j,t)\right) \quad (43)$$

Zone-II (0 ≤ y ≤ k) (Saffman Dusty fluid)

$$u_{2_t}=\frac{Ge(t)}{r_2}+\frac{r_1}{r_2}\frac{\sum_{j=1}^{N} V^*{}_{ij} u_2(y_j,t)}{Re}-\frac{R*r_1}{r_2}\frac{\left(u_2(y_j,t)-u_p(y_j,t)\right)}{Re} \quad (44)$$

$$u_{p_t}=\frac{R*r_3*r_1}{r_2}\frac{\left(u_2(y_j,t)-u_p(y_j,t)\right)}{Re} \quad (45)$$

Thus, equations are reduced into a system of ordinary differential equations in time, that is, for *i=1, 2, 3…, N*, and the system is solved by the robust four-step third-order SSP RK43 scheme. The velocities and microrotation in both Zones are obtained as follows:

At first - the step for i=1,2,3…,n

Zone-I ($-k \le y \le 0$) (micropolar fluid):

$$u_{1_1}=u_{1_0}+\frac{\Delta t}{2}\left(Ge(t)+\frac{n_1}{Re}\left(\sum_{j=1}^{N} U^*{}_{ij} M_{*_0}(y_j,t)\right)+\frac{(n_1+1)}{Re}\left(\sum_{j=1}^{N} V^*{}_{ij} u_{1_0}(y_j,t)\right)\right) \quad (46)$$

$$M_{*1}=M_{*0}+\frac{\Delta t}{2}\left(\frac{(n_1+2)}{2Re}\left(\sum_{j=1}^{N} V^*{}_{ij} M_{*_0}(y_j,t)\right)-\frac{n_1}{Re}\left(2M_{*_0}+\sum_{j=1}^{N} U^*{}_{ij} u_{1_0}(y_j,t)\right)\right) \quad (47)$$

Zone-II (0 ≤ y ≤ k) (Saffman dusty fluid):

$$u_{2_1}=u_{2_0}+\frac{\Delta t}{2}\left(\frac{Ge(t)}{r_2}+\frac{r_1}{r_2}\frac{\sum_{j=1}^{N} V^*{}_{ij} u_{2_0}(y_j,t)}{Re}-\frac{R*r_1}{r_2}\frac{\left(u_{2_0}(y_j,t)-u_{p_0}(y_j,t)\right)}{Re}\right) \quad (48)$$

$$u_{p_1}=u_{p_0}+\frac{\Delta t}{2}\left(\frac{R*r_3*r_1}{r_2}\frac{\left(u_{2_0}(y_j,t)-u_{p_0}(y_j,t)\right)}{Re}\right) \quad (49)$$

At the first step of the method, the conditions (13)-(23)are regarded favorably.

At the second step for i=1,2,3…,n:

Zone-I ($-k \le y \le 0$) (micropolar fluid):

$$u_{1_2}=u_{1_1}+\frac{\Delta t}{2}\left(Ge(t)+\frac{n_1}{Re}\left(\sum_{j=1}^{N} U^*{}_{ij} M_{*_1}(y_j,t)\right)+\frac{(n_1+1)}{Re}\left(\sum_{j=1}^{N} V^*{}_{ij} u_{1_1}(y_j,t)\right)\right) \quad (50)$$

$$M_{*2}=M_{*1}+\frac{\Delta t}{2}\left(\frac{(n_1+2)}{2Re}\left(\sum_{j=1}^{N} V^*{}_{ij} M_{*_1}(y_j,t)\right)-\frac{n_1}{Re}\left(2M_{*_1}+\sum_{j=1}^{N} U^*{}_{ij} u_{1_1}(y_j,t)\right)\right) \quad (51)$$

Zone-II (0 ≤ y ≤ k) (Saffman dusty fluid):

$$u_{2_2}=u_{2_1}+\frac{\Delta t}{2}\left(\frac{Ge(t)}{r_2}+\frac{r_1}{r_2}\frac{\sum_{j=1}^{N} V^*{}_{ij} u_{2_1}(y_j,t)}{Re}-\frac{R*r_1}{r_2}\frac{\left(u_{2_1}(y_j,t)-u_{p_1}(y_j,t)\right)}{Re}\right) \quad (52)$$

$$u_{p_2} = u_{p_1} + \frac{\Delta t}{2}\left(\frac{R*r_3*r_1}{r_2}\frac{\left(u_{2_1}(y_j,t)-u_{p_1}(y_j,t)\right)}{Re}\right) \quad (53)$$

At the second step of the method, the conditions (13)-(23) are regarded favorably.

At the third step for i=1,2,3…, n

Zone-I ($-k \le y \le 0$) (micropolar fluid):

$$u_{1_3} = \frac{2u_{1_0}}{3} + \frac{u_{1_2}}{3} + \frac{\Delta t}{6}\left(Ge(t) + \frac{n_1}{Re}\left(\sum_{j=1}^{N} U^*{}_{ij} M_{*_2}(y_j,t)\right) + \frac{(n_1+1)}{Re}\left(\sum_{j=1}^{N} V^*{}_{ij} u_{1_2}(y_j,t)\right)\right) \quad (54)$$

$$M_{*_3} = \frac{2M_{*_0}}{3} + \frac{M_{*_2}}{3} + \frac{\Delta t}{6}\left(\frac{(n_1+2)}{2Re}\left(\sum_{j=1}^{N} V^*{}_{ij} M_{*_2}(y_j,t)\right) - \frac{n_1}{Re}\left(2M_{*_2} + \sum_{j=1}^{N} U^*{}_{ij} u_{1_2}(y_j,t)\right)\right) \quad (55)$$

Zone-II (0 ≤ y ≤ k) (Saffman dusty fluid):

$$u_{2_3} = \frac{2u_{2_0}}{3} + \frac{u_{2_2}}{3} + \frac{\Delta t}{6}\left(\frac{Ge(t)}{r_2} + \frac{r_1}{r_2}\frac{\sum_{j=1}^{N} V^*{}_{ij} u_{2_2}(y_j,t)}{Re} - \frac{R*r_1}{r_2}\frac{\left(u_{2_2}(y_j,t)-u_{p_2}(y_j,t)\right)}{Re}\right) \quad (56)$$

$$u_{p_3} = \frac{2u_{p_0}}{3} + \frac{u_{p_2}}{3} + \frac{\Delta t}{6}\left(\frac{R*r_3*r_1}{r_2}\frac{\left(u_{2_2}(y_j,t)-u_{p_2}(y_j,t)\right)}{Re}\right) \quad (57)$$

At the third step of the method, the conditions (13)-(23) are once again regarded favourably.

At the fourth step for i=1,2,3…,n:

Zone-I ($-k \le y \le 0$) (micropolar fluid):

$$u_1 = u_{1_3} + \frac{\Delta t}{2}\left(Ge(t) + \frac{n_1}{Re}\left(\sum_{j=1}^{N} U^*{}_{ij} M_{*_3}(y_j,t)\right) + \frac{(n_1+1)}{Re}\left(\sum_{j=1}^{N} V^*{}_{ij} u_{1_3}(y_j,t)\right)\right) \quad (58)$$

$$M_* = M_{*_3} + \frac{\Delta t}{2}\left(\frac{(n_1+2)}{2Re}\left(\sum_{j=1}^{N} V^*{}_{ij} M_{*_3}(y_j,t)\right) - \frac{n_1}{Re}\left(2M_{*_3} + \sum_{j=1}^{N} U^*{}_{ij} u_{1_3}(y_j,t)\right)\right) \quad (59)$$

Zone-II (0 ≤ y ≤ k) (Saffman dusty fluid):

$$u_2 = u_{2_3} + \frac{\Delta t}{2}\left(\frac{Ge(t)}{r_2} + \frac{r_1}{r_2}\frac{\sum_{j=1}^{N} V^*{}_{ij} u_{2_3}(y_j,t)}{Re} - \frac{R*r_1}{r_2}\frac{\left(u_{2_3}(y_j,t)-u_{p_3}(y_j,t)\right)}{Re}\right) \quad (60)$$

$$u_p = u_{p_3} + \frac{\Delta t}{2}\left(\frac{R*r_3*r_1}{r_2}\frac{\left(u_{2_3}(y_j,t)-u_{p_2}(y_j,t)\right)}{Re}\right) \quad (61)$$

At the fourth step of the method, the conditions (13)-(23) are also regarded favourably. Hence the fluid (linear) velocity and angular velocity (Eringen microrotation) profiles i. e. u_1, M_* of micropolar fluid in Zone-I and also the fluid velocity (linear) and particle velocity components i.e. u_2, u_p for Saffman dusty fluid in Zone-II can be numerically obtained at the fourth step of MCB-DQM.

4.Results and Interpretation

Under two separate flow schemes, the unidirectional unstable flow of two immiscible (i. e. Saffman dusty and Eringen micropolar fluids) attributable to the time-dependent pressure gradient has been simulated with a novel MCB-DQM algorithm. To obtain robust solutions, traditional no-slip and hyper-stick conditions are assumed at the boundaries. The two-fluid flow coupled problem in the corresponding Zones with stable interfaces have been numerically solved, and

velocity, micro-rotation, and dust phase profiles of the respective fluids and dust particles have been obtained. The results are discussed as follows.

4.1 Results and analysis of immiscible dusty and micropolar fluid flow:

Figure 2-Figure *21* visualize the evolution in fluid and dust particle-phase velocities and also micro-rotation (angular velocity) distributions in the respective dusty and micropolar zones with variation in key control parameters featured in the mathematical model i. e. *Reynolds number, particulate concentration parameter, applied pressure gradients, density ratio, viscosity ratio, and time*. It is evident that the linear velocity profiles for the dust (zone I) and fluid phase in both Zones are *parabolic*, and the curvature of micropolar angular velocity (microrotation) is lower than dusty one. Furthermore, the curvature of velocity and micro-rotation profiles for the *periodic pressure gradient* case is smaller than the *decaying pressure gradient* and the curvature for constant pressure gradient is larger than that computed for the decaying pressure gradient case. **Figure 2** and **Figure 12** exhibits the change in fluid and particle velocities and micro-rotation with varying times when a constant pressure gradient is applied. It is noted that, with rising time, the velocities are growing in both Zones and micro-rotation profile magnitude is accentuated in the micropolar liquid Zone. **Figure *3*** and **Figure 13** show that the dust particle, dusty fluid, and micropolar linear velocities, and also microrotation (angular velocity) are all *pulsating* since the flow is induced by the periodic pressure gradient and never achieves the steady state. Hence the velocities increase when $0 < t \leq \pi/2$, decrease when $\pi/2 < t \leq 3\pi/2$ and further increase with $3\pi/2 < t \leq 5\pi/2$. **Figure *4*** and **Figure 14** reveal that the fluid and particle velocities and micro-rotation increase initially in the respective Zones then decrease with greater elapse in time and eventually approach zero as time is enhanced when the applied periodic pressure gradient generates the flow. It can be noted from **Figure *11*** **and Figure 21** that the linear velocity (micropolar fluid, dusty fluid, and dust particle) and micro-rotation profiles increase with an increment in the pressure gradient. It may be observed from **Figure *5*** and

Figure *15* that elevation in Reynolds number enhances both the fluids and particle velocities and micro-rotation magnitudes, owing to the increase in inertial force contribution (relative to viscous force) for *all three pressure gradient cases*- i.e. applied constant, periodic, and decaying pressure gradients. However, the variations in the velocities are larger in magnitude in the dusty fluid Zone than in the micropolar liquid Zone, indicating the greater sensitivity of Saffman dusty fluid to inertial effects. An increase in the micropolar parameter reduces the velocity profiles for fluid and dust particles (via coupling in the conservation equations) in both Zones and also suppresses microrotation profiles in the lower Zone for all three applied pressure gradients (see **Figure *6*** and **Figure 16**). Stronger micropolarity of the micropolar liquid, therefore, achieves a notable damping effect in both zones. It is worth mentioning that the micropolar parameter while unique to micropolar fluid in the lower Zone exerts a significant (no-trivial) influence on the upper zone (Saffman dusty fluid) via the appropriate coupling terms in the angular momentum (micro-rotation) conservation equation. This markedly modifies the velocity of dust particles and dusty fluid, although there is no fluid mechanical framework in Saffman's model for simulating microstructural spin. The elegance of Eringen's theory is therefore again emphasized since it not only generalizes Navier-Stokes (Newtonian) viscous hydrodynamics but also provides a coupling mechanism to other fluid models via the inclusion of mixed derivative coupling terms in the differential balance equations. Micropolar theory features an additional Eringen vortex viscosity and also allows the relative effect of rotation to linear motion to

be simulated through the gyratory motions in the micro-rotation vector. The micropolar effect is also removable by prescribing vanishing values to the micropolar parameter, another advantage of micropolar fluid mechanics.

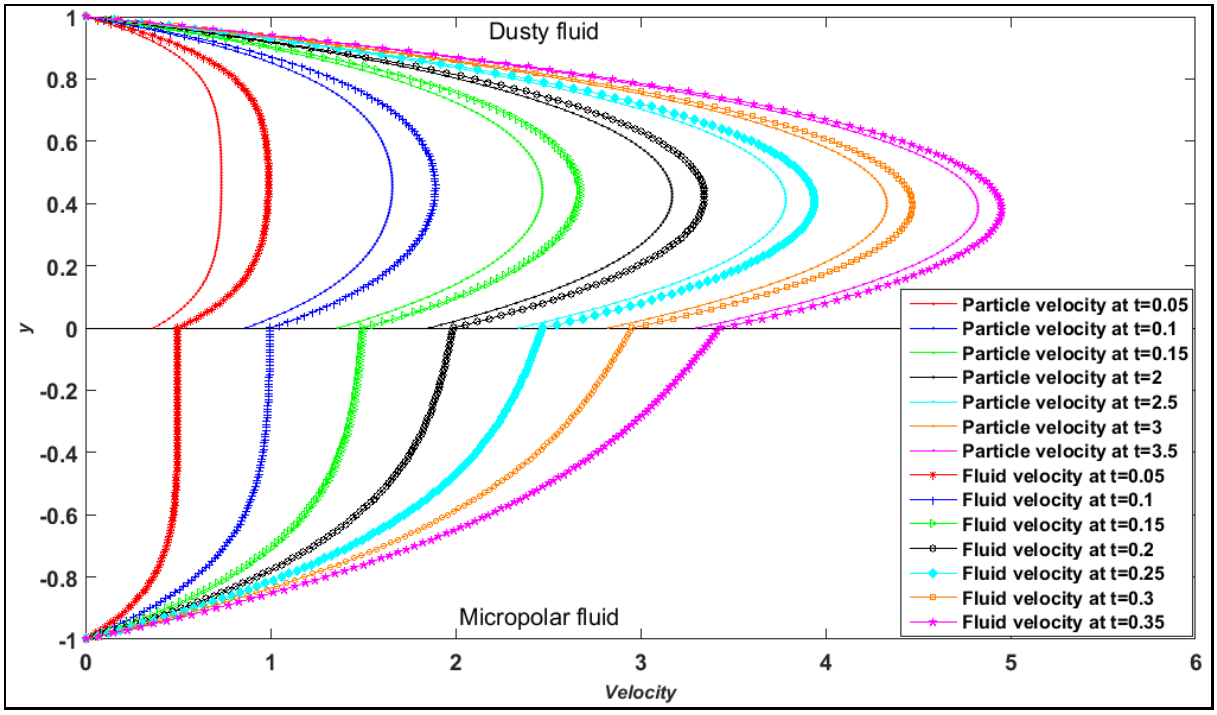

Figure 2: Velocity profiles of fluids under the scheme with varying time and constant pressure gradient Ge=10, when Re=2, R=0.5, r_1=0.5, r_2=0.5, r_3=300, and η_1=0.5

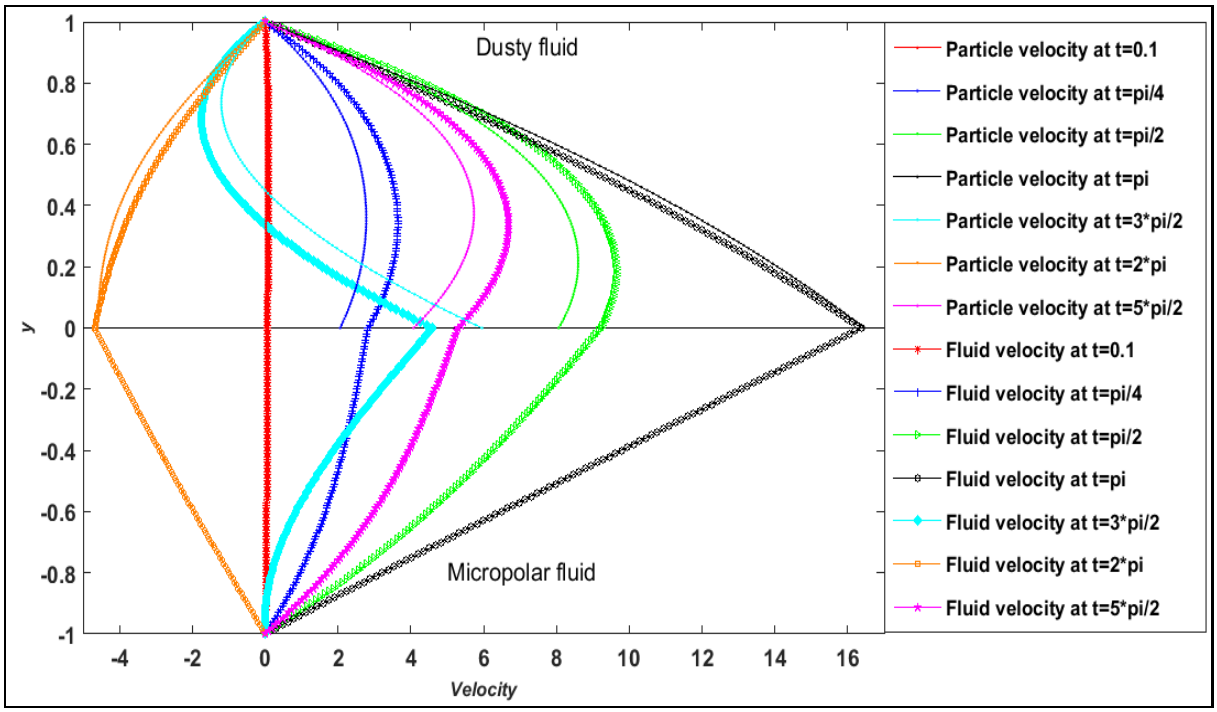

Figure 3:Velocity profiles of fluids under the scheme with varying time and periodic pressure gradient when Re=2, R=0.5, r_1=0.5, r_2=0.5, r_3=300, and η_1=0.5

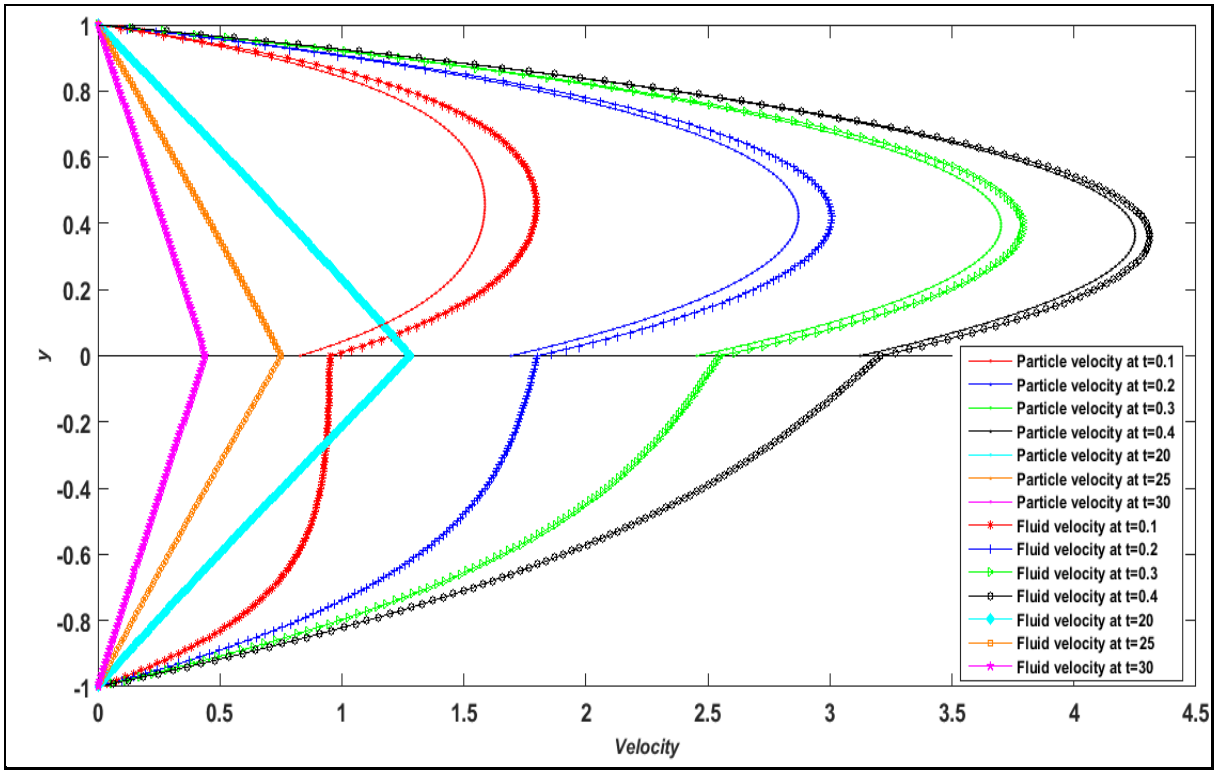

Figure 4: Velocity profiles of fluids under the scheme with varying time and decaying pressure gradient when Re=2, R=0.5, τ_1=0.5, τ_2=0.5, τ_3=300, and η_1=0.5

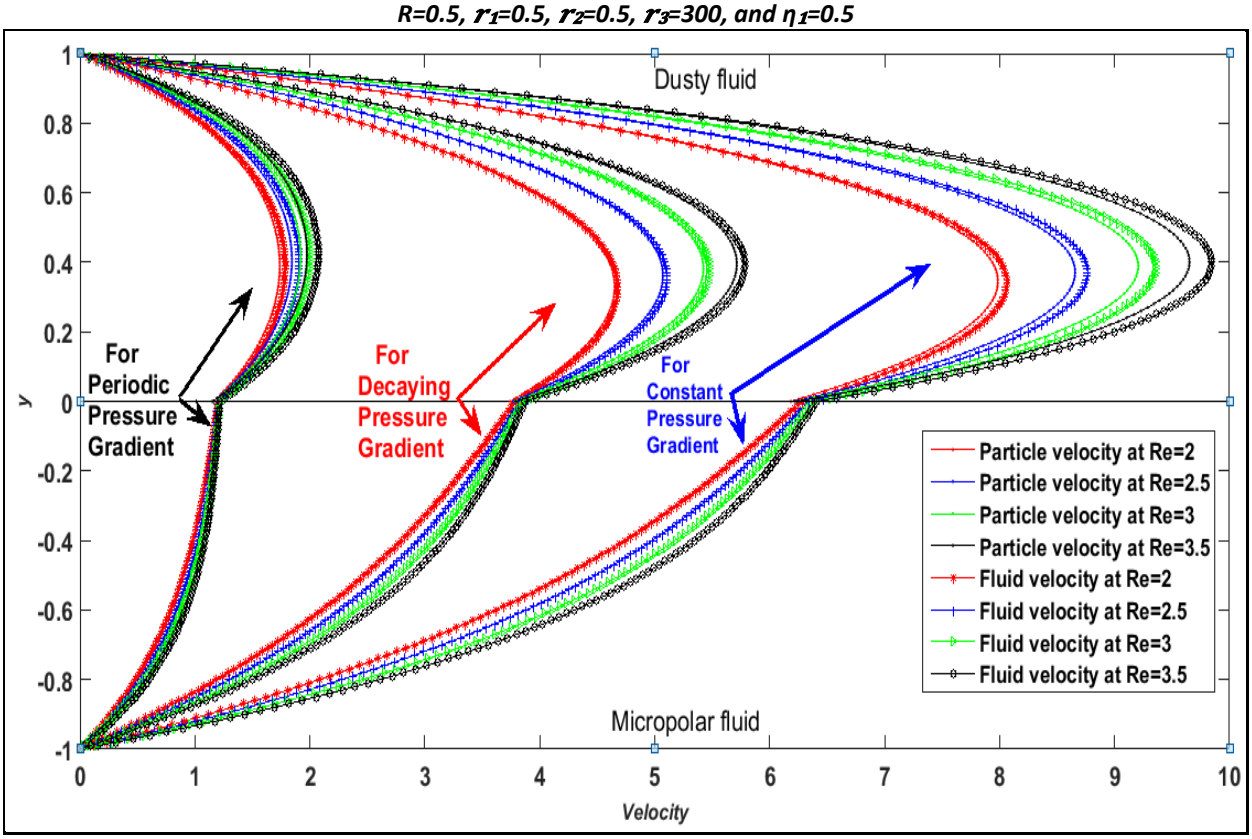

Figure 5:Velocity profiles of fluids under the scheme with varying Reynolds number and applied pressure gradient when t=0.5, R=0.5, τ_1=0.5, τ_2=0.5, τ_3=300, and η_1=0.5

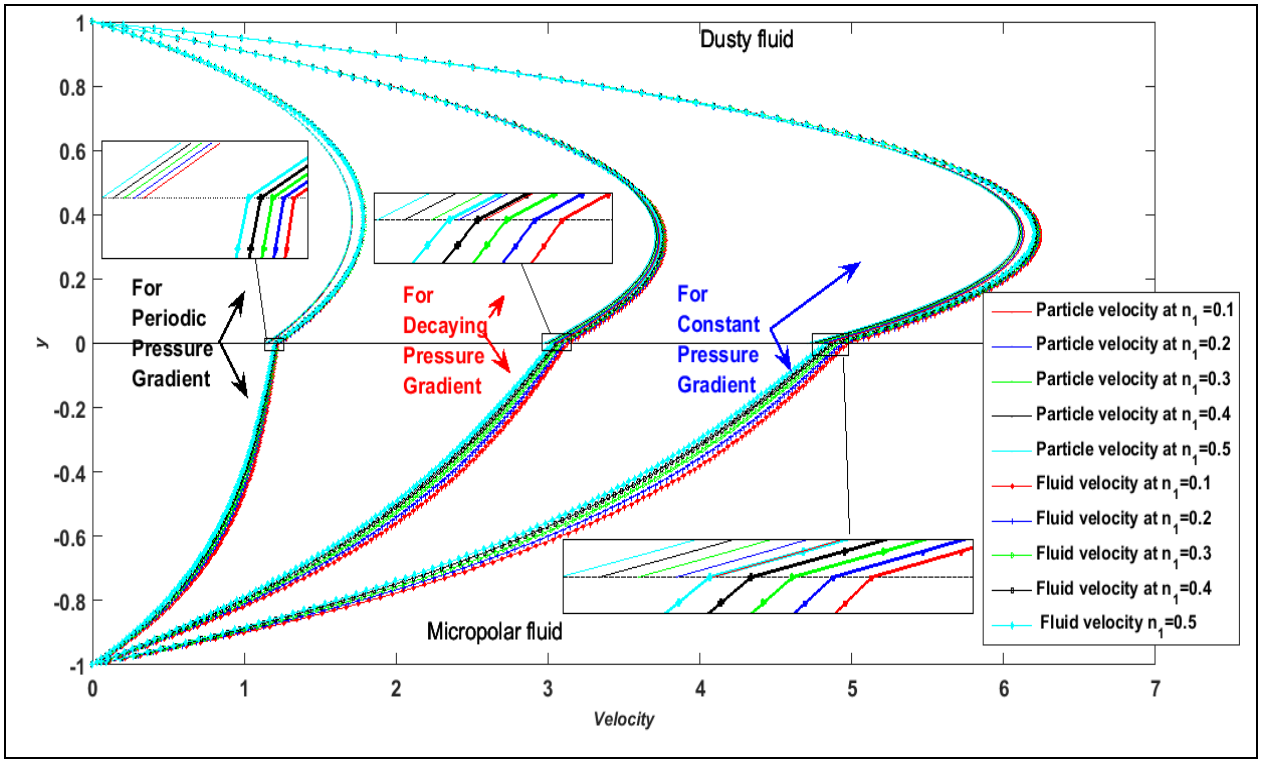

Figure 6: Velocity profiles of fluids under the scheme with varying micropolar parameters (n_1) and applied pressure gradient (Ge) when, t=0.5, R=0.5, r_1=0.5, r_2=0.5, r_3=300, and Re=2

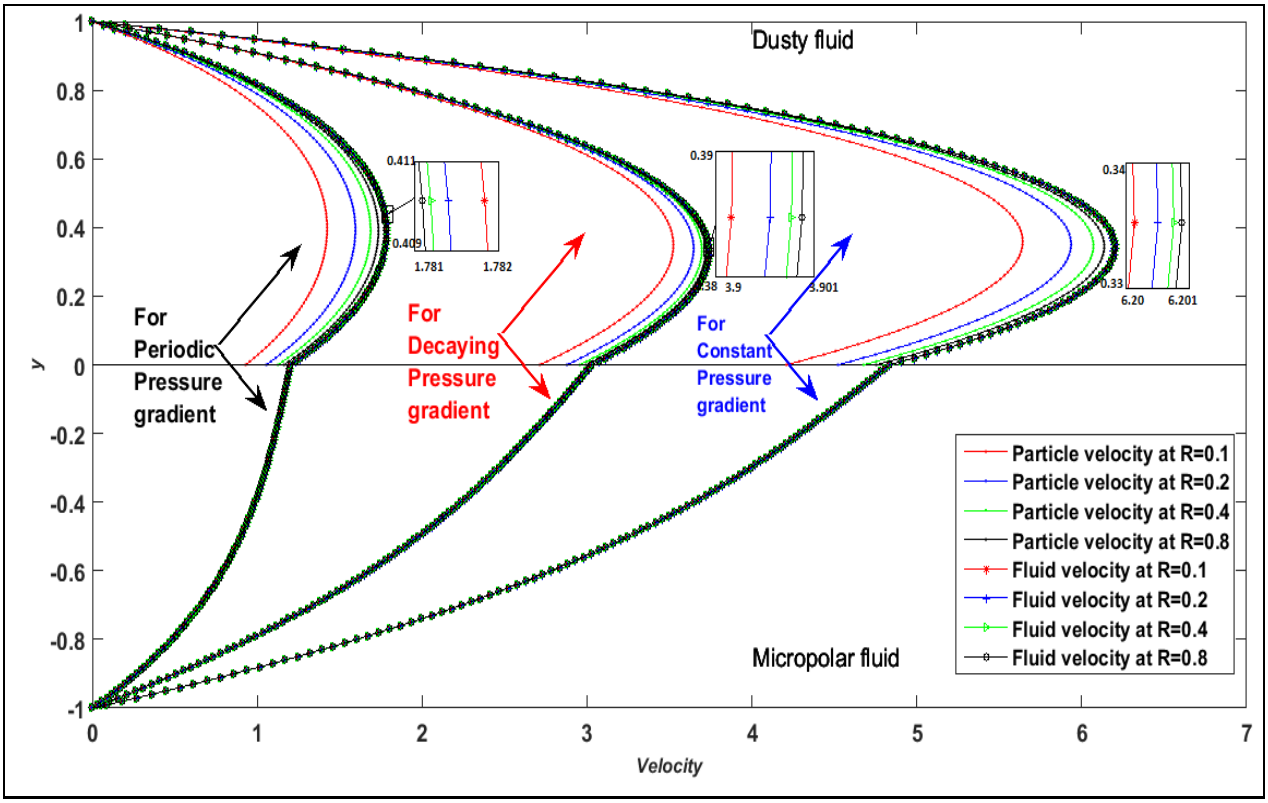

Figure 7: Velocity profiles of fluids under the scheme with varying particle concentration parameter and applied pressure gradient when t=0.5, Re=2, r_1=0.5, r_2=0.5, r_3=300, and η_1=0.5

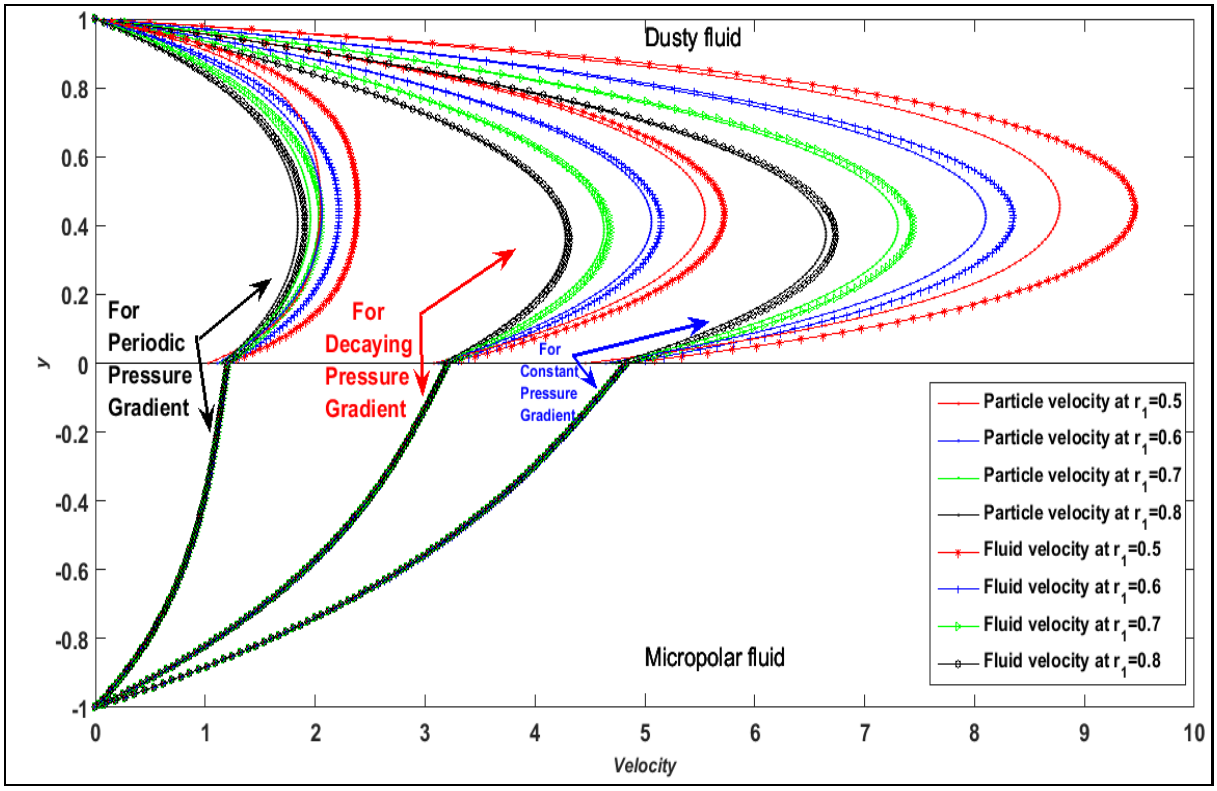

Figure 8: Velocity profiles of fluids under the scheme with varying ratio of viscosities and applied pressure gradient when t=0.5, Re=2, R=0.5, r_2=0.5, r_3=300, and η_1=0.5

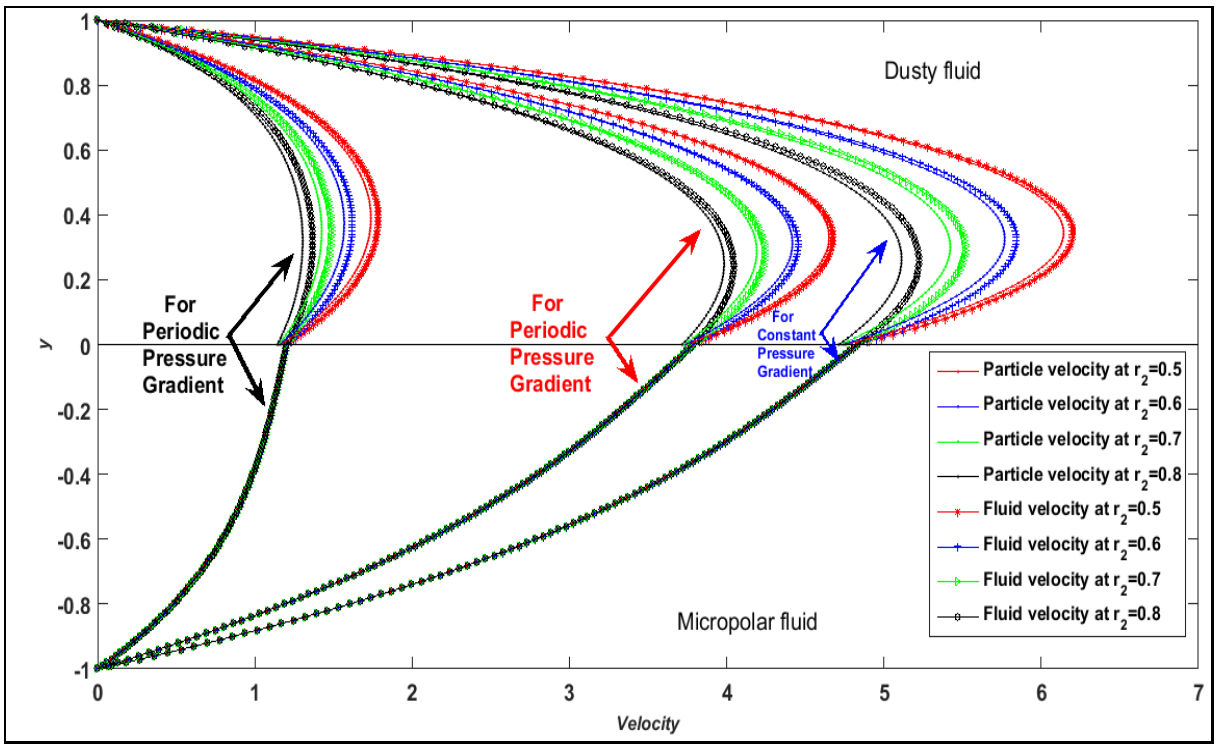

Figure 9:Velocity profiles of fluids under the scheme with varying ratio of densities and applied pressure gradient when, t=0.5, Re=0.5, R=0.5, r_1=0.5, r_3=300, and η_1=0.5

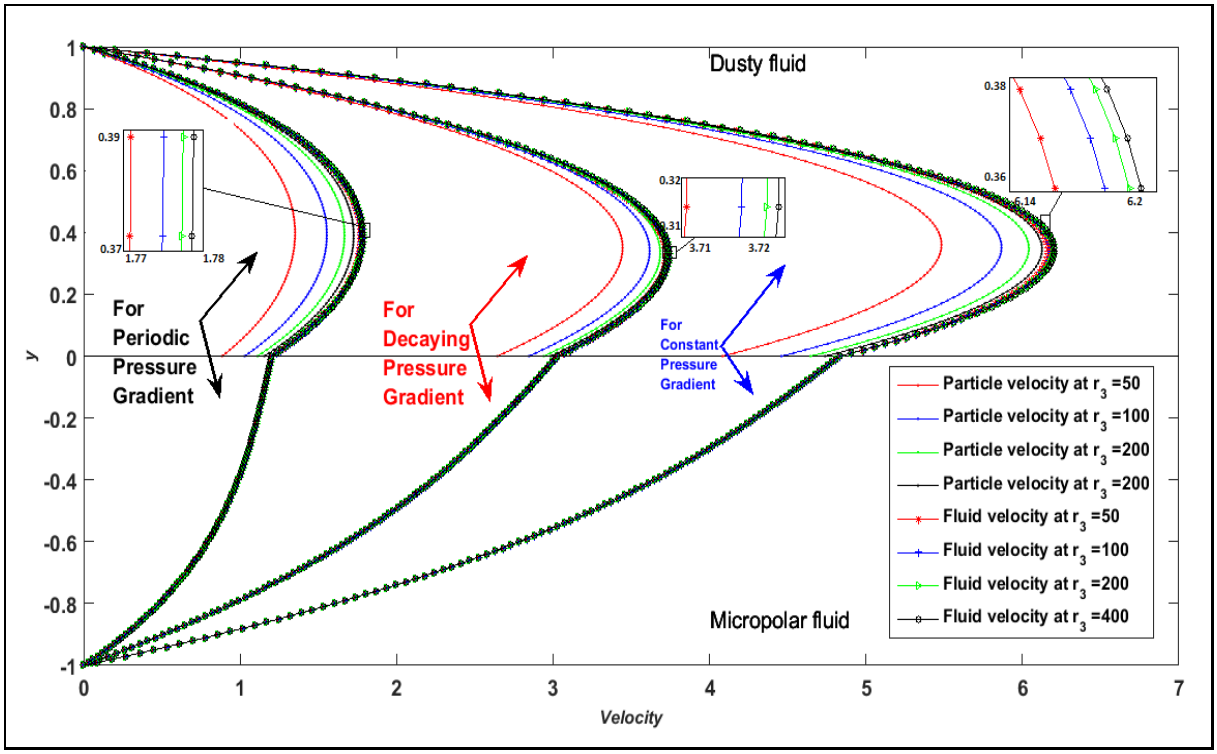

Figure 10: Velocity profiles of fluids under the scheme with varying r_3 and applied pressure gradient when t=0.5, Re=2, R=0.5, r_1=0.5, r_2=0.5, and η_1=0.5

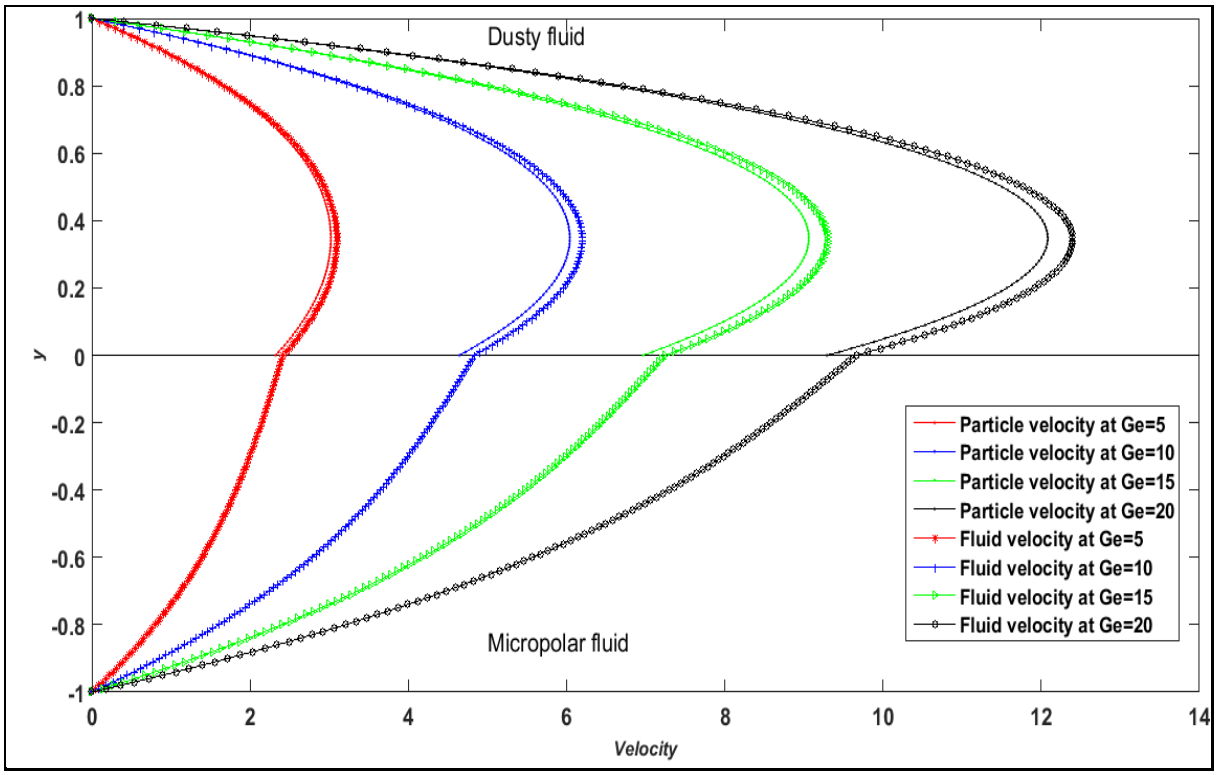

Figure 11:Velocity profiles of fluids under the scheme with varying constant pressure gradient when, t=0.5, Re=2, R=0.5, r_1=0.5, r_2=0.5, r_3=300, and η_1 = 0.5.

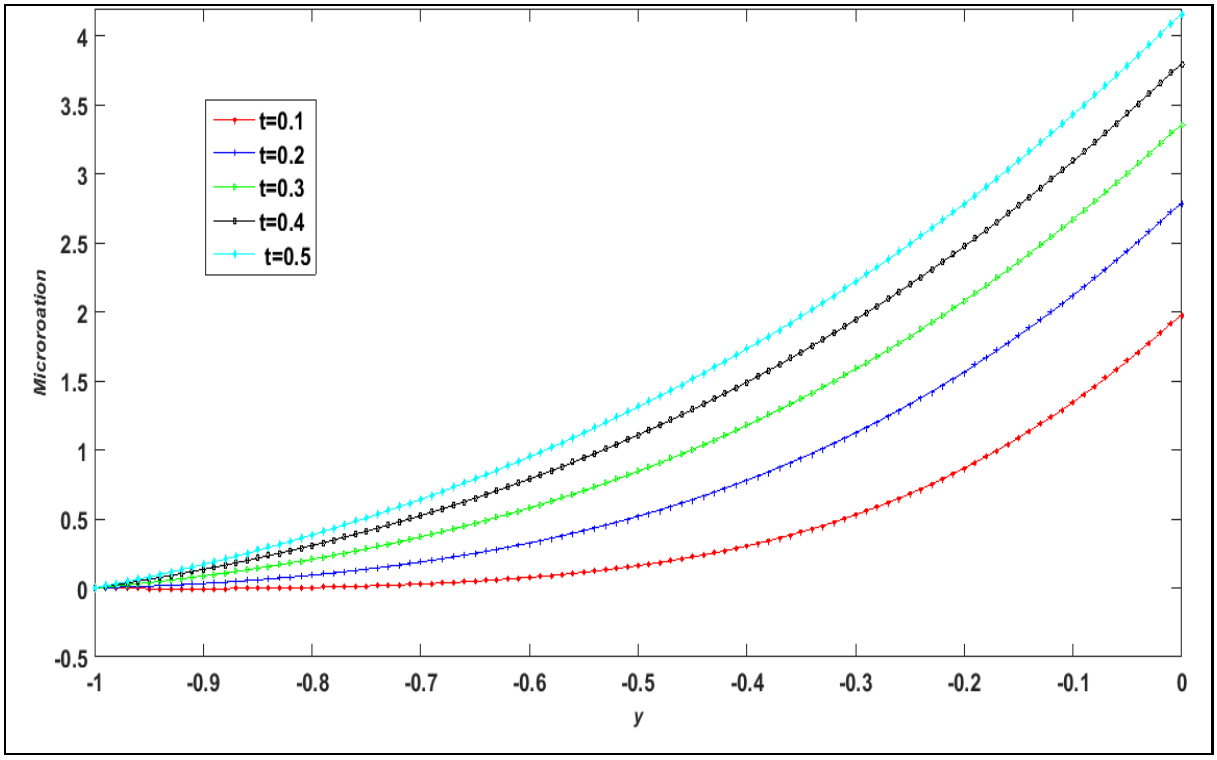

Figure 12: Micro-rotation profiles of micropolar fluid under the scheme with varying time and constant pressure gradient Ge=10, when Re=2, R=0.5, r_1=0.5, r_2=0.5, r_3=300, and η_1=0.5

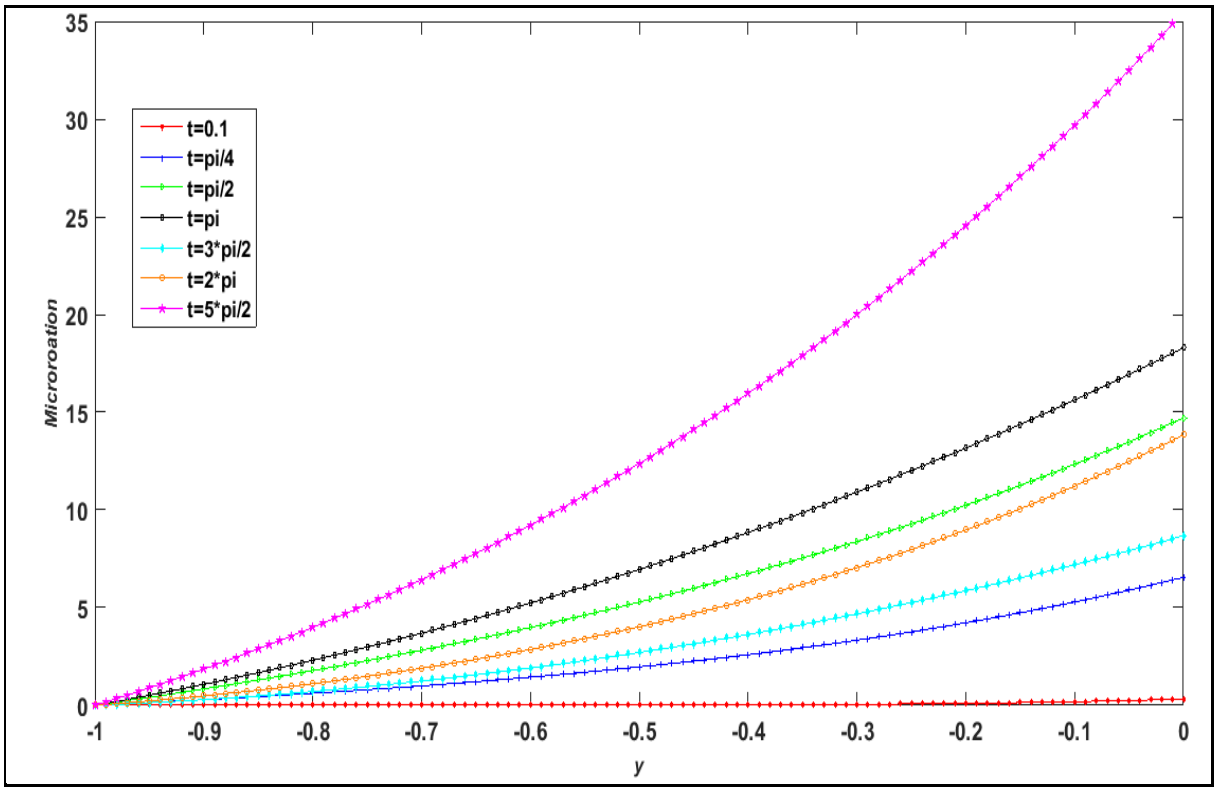

Figure 13: Micro-rotation profiles for micropolar fluid under the scheme with varying time and periodic pressure gradient *Ge=10*, when Re=2, R=0.5, r_1=0.5, r_2=0.5, r_3=300, and η_1=0.5

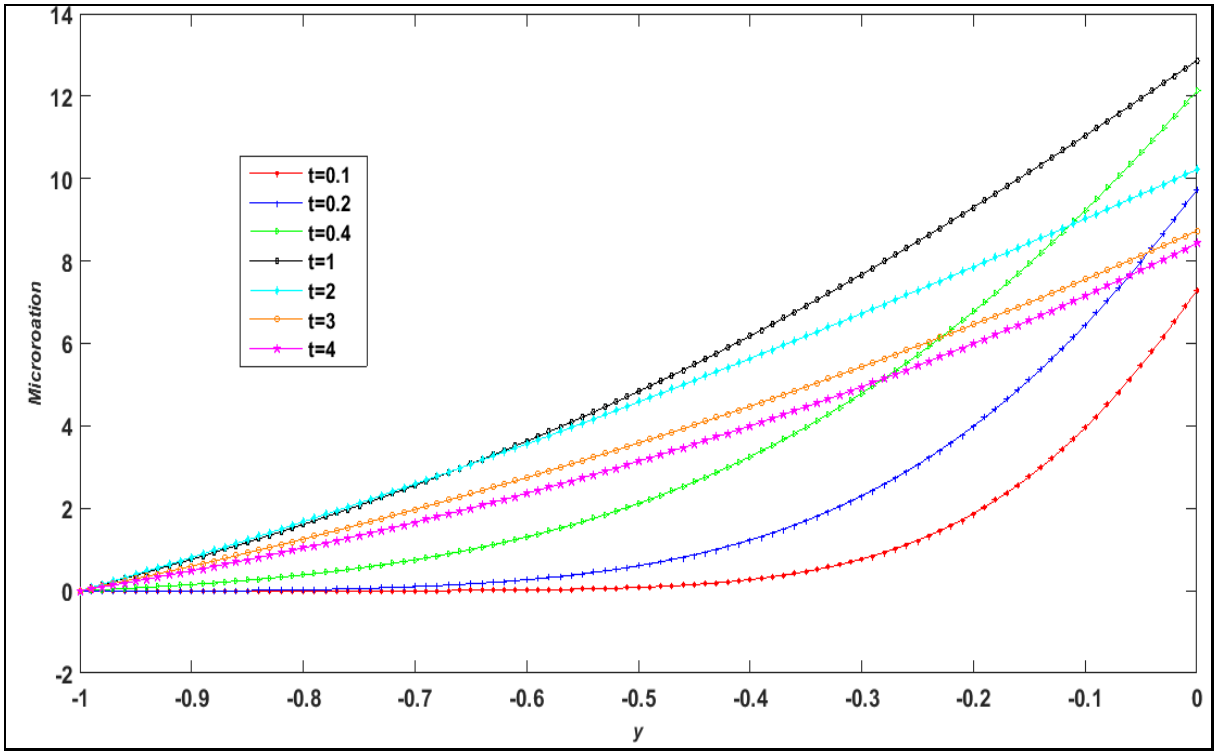

Figure 14: Micro-rotation profiles of micropolar fluid under the scheme with varying time and periodic pressure gradient *Ge*=10, when *Re=2, R=0.5*, r_1=0.5, r_2=0.5, r_3=300, and η_1=0.5

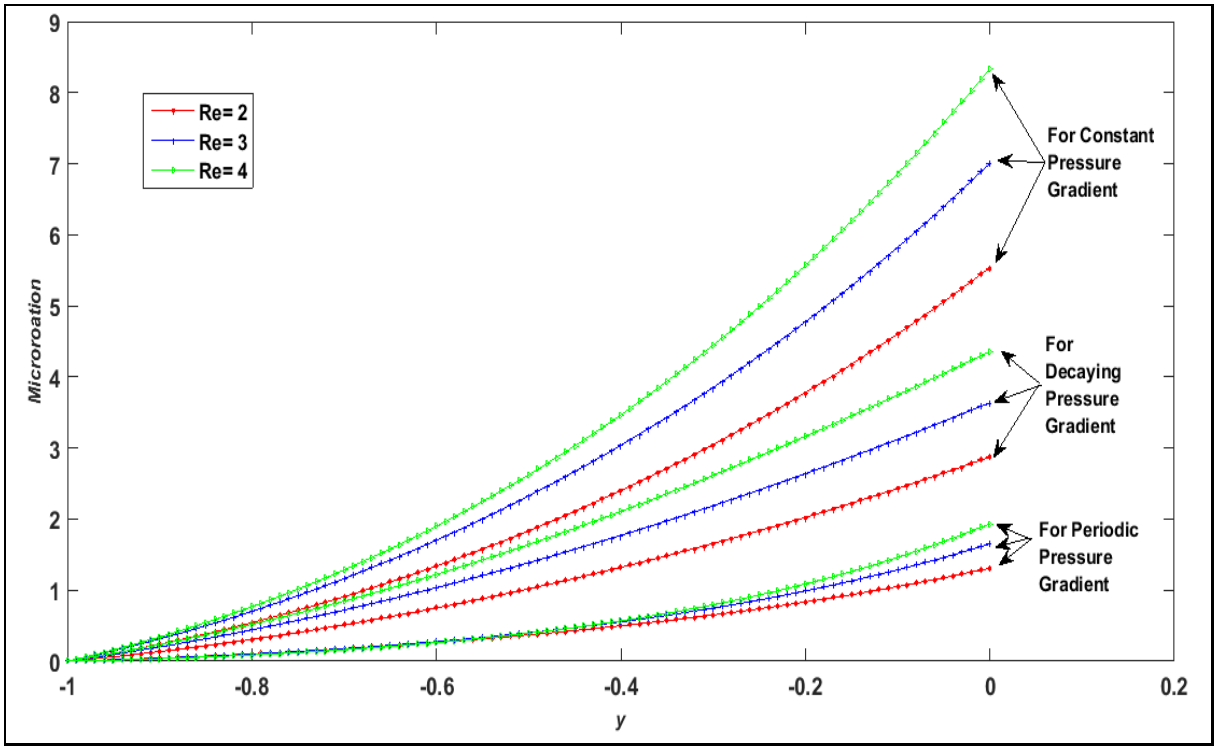

Figure 15: Micro-rotation profiles of Micro-polar fluid under the scheme with varying Reynolds number and applied pressure gradient when, t=0.5, R=0.5, r_1=0.5, r_2=0.5, r_3=300, and η_1=0.5

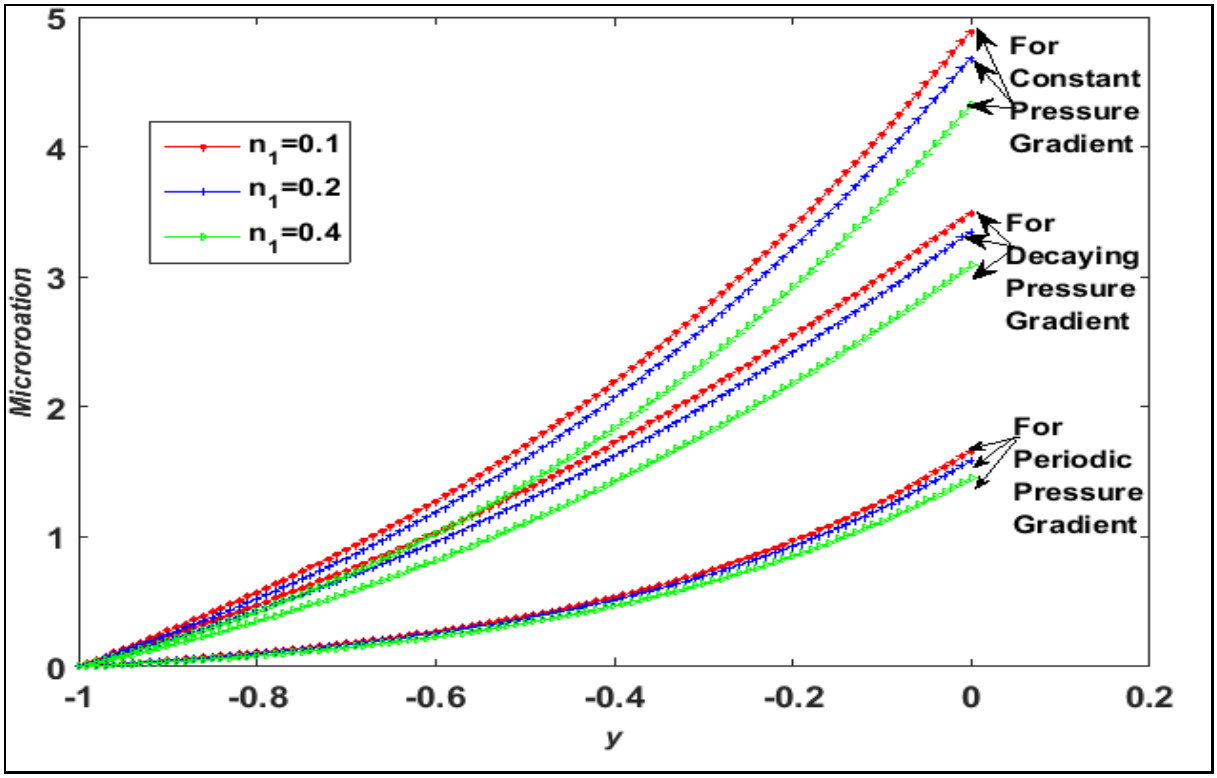

Figure 16: Micro-rotation profiles of micropolar fluid under scheme with varying micropolar parameter (η_1) and applied pressure gradient when, *t=0.5, R=0.5*, r_1=0.5, r_2=0.5, r_3=300 and *Re=2*

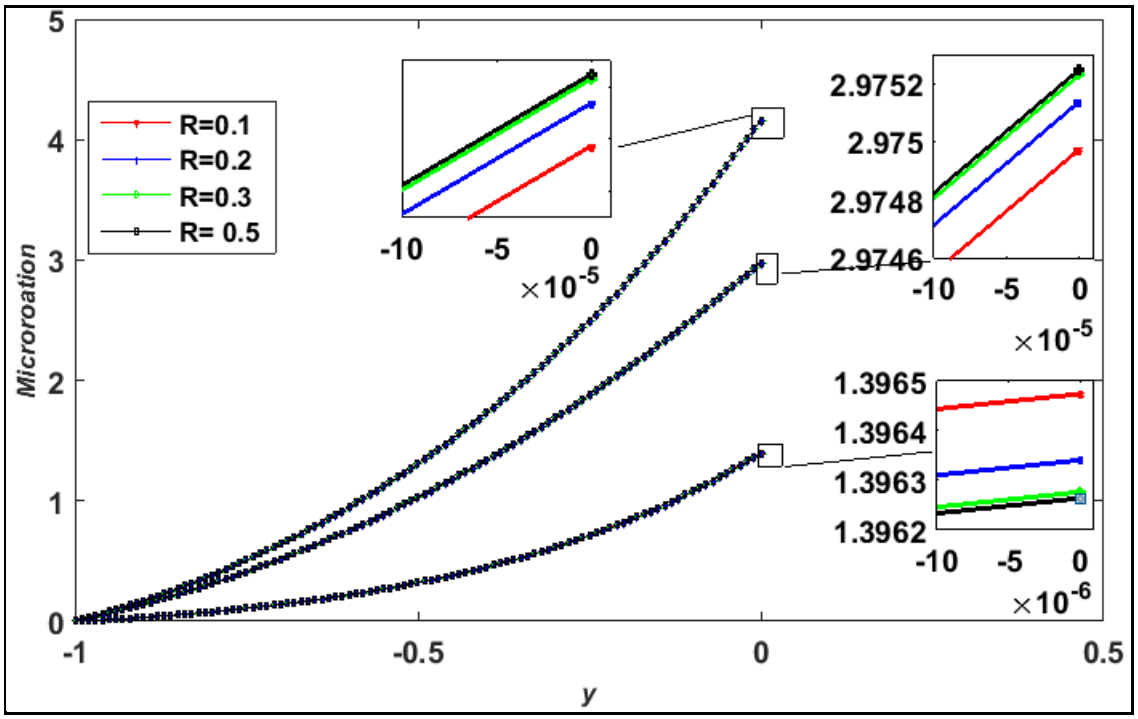

Figure 17: Micro-rotation profiles of micropolar fluid for the scheme with varying particle concentration parameter *(R)* and applied pressure gradient when *t=0.5, Re=2*, r_1=0.5, r_2=0.5, r_3=300, and η_1=0.5

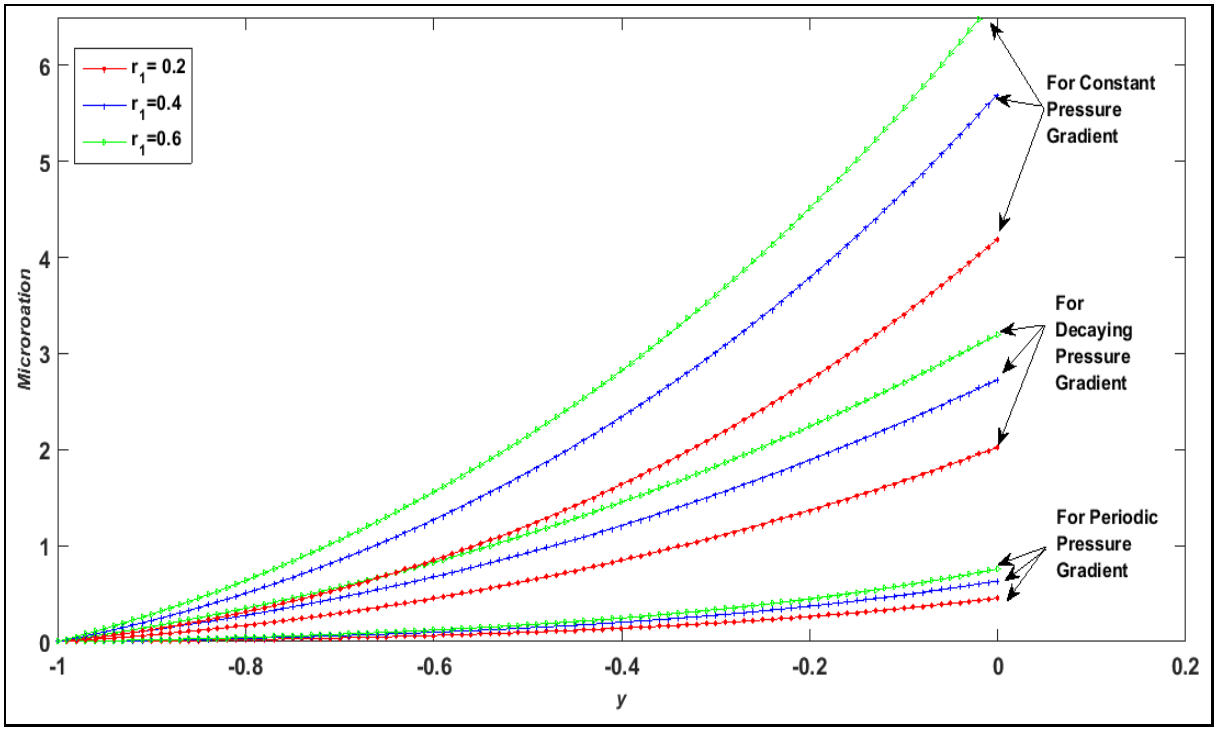

Figure 18: Micro-rotation profiles of micropolar fluid under scheme with varying ratio of viscosities and applied pressure gradient when *t=0.5, Re=2, R=0.5, r_2=0.5, r_3=300* and η_1=0.5

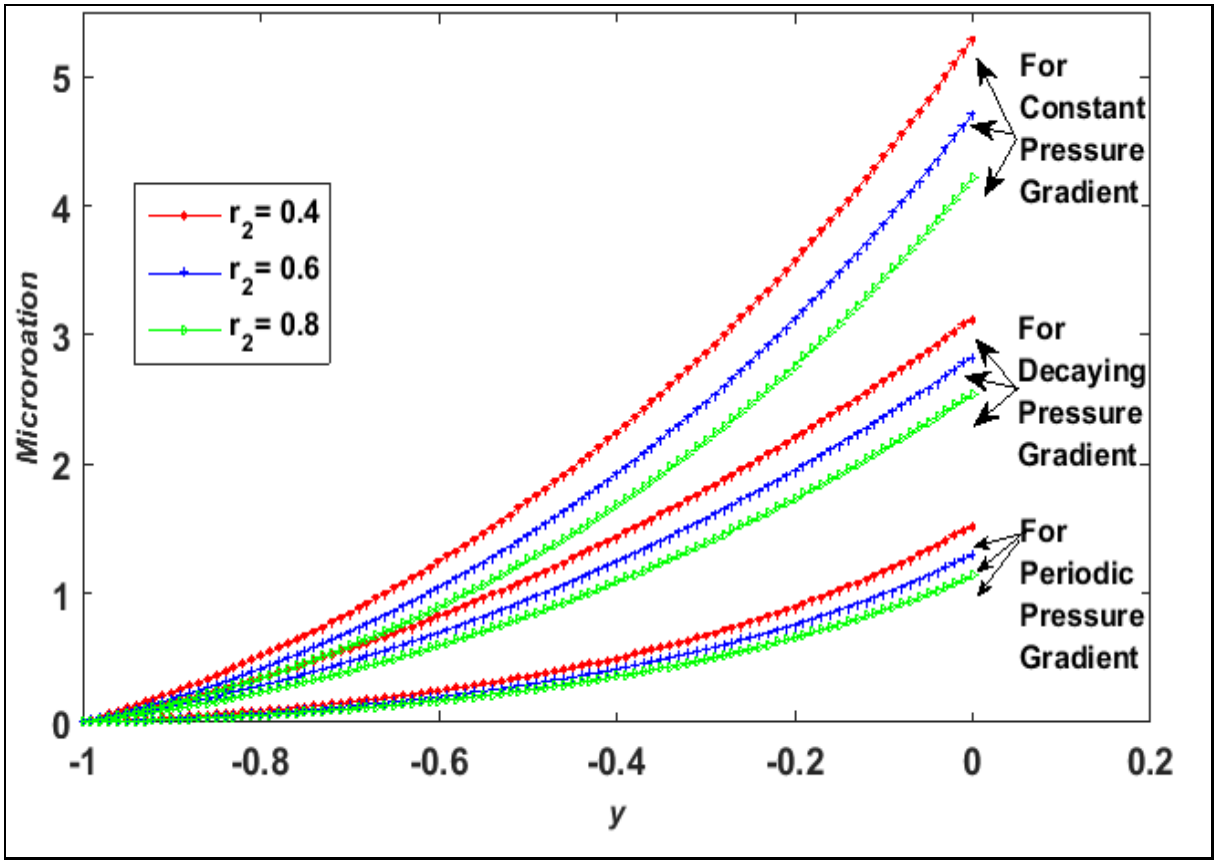

Figure 19: Micro-rotation profiles of micropolar fluid under scheme with varying ratio of densities (r_2) and applied pressure gradient when, *t=0.5, Re=2, R = 0.5, r_1=0.5, r_3=300, and η_1=0.5*

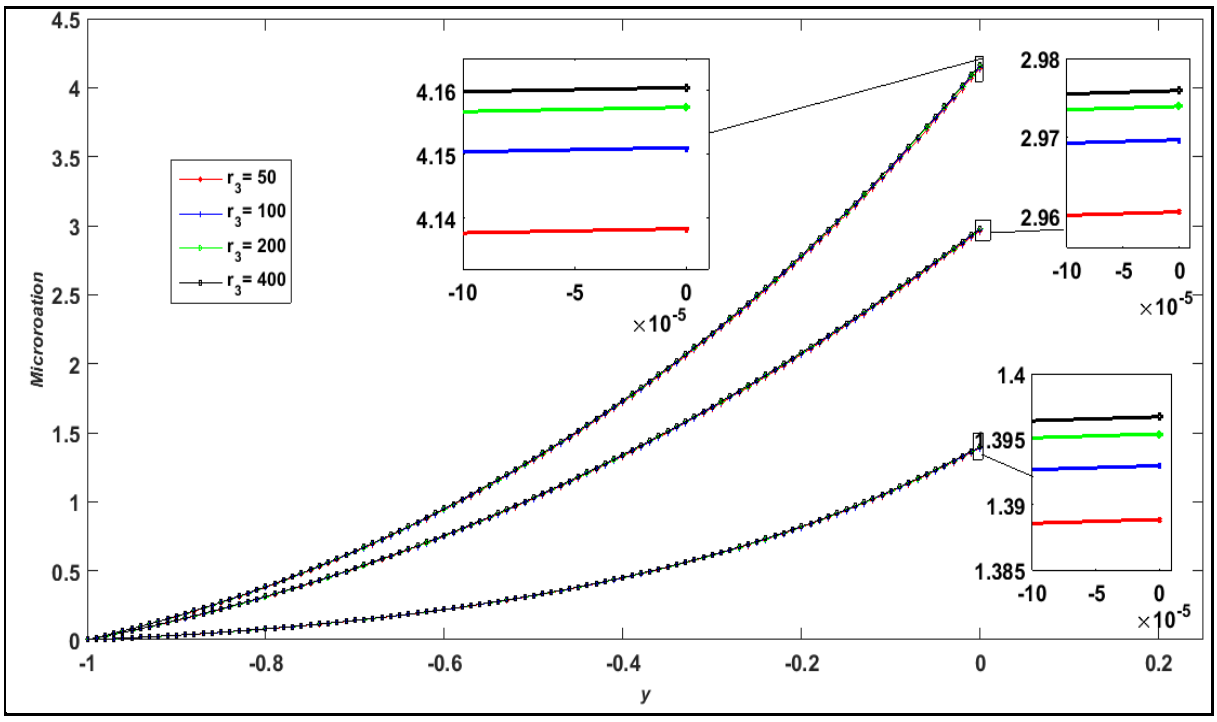

Figure 20: Micro-rotation profiles of micropolar fluid under the scheme with varying *ratio of the density of fluid and dust particles* (r_3) **and applied pressure gradient** ***when t=0.5, Re=2, R=0.5, r_1=0.5, r_2=0.5, and η_1=0.5***

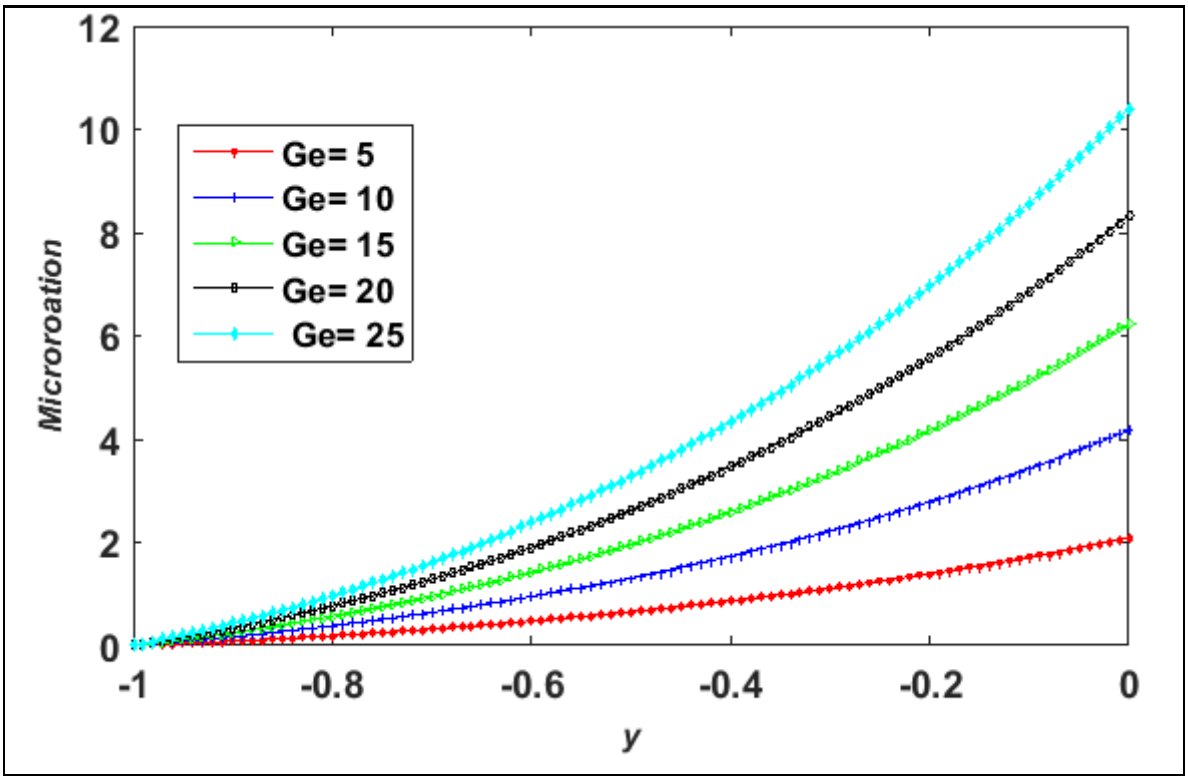

Figure 21: Micro-rotation profiles of micropolar fluid under the scheme with varying constant pressure gradient when, ***t=0.5, Re=2, R=0.5, r_1= 0.5, r_2= 0.5, r_3=300***, **and η_1=0.5.**

It is noted from **Figure *7*** and **Figure 17** that dust particle velocity *increases significantly* with the enhancement of particle concentration parameter, and a very slight increase in dusty fluid velocity and micro-rotation component (Eringen angular velocity of micro-elements) is observed for constant and decaying applied pressure gradients. Hence there is no substantial effect of particle concentration parameter on micropolar fluid velocity. It is also judicious to note that dusty fluid velocity and micro-rotation decrease marginally when a periodic pressure gradient is applied. An increase in the viscosity ratio r_1 and density ratio r_2 manifests in an increase in the viscosity and density of the dusty fluid Zone. In view of this, for all three applied pressure gradients, a significant decline in dust particle and fluid velocity (Zone-II) is computed whereas there is no tangible alteration in the micropolar fluid velocity (Zone-I) with an increase in r_1 and r_2 (see **Figure *8*** and **Figure *9***). It is also observed from **Figure 18** and **Figure *19*** for all three applied pressure gradients that as the ratio r_1 enhances, the micro-rotation profile increases significantly; however, when r_2 rises, the micro-rotation profile decreases significantly. Acceleration in gyratory motions of microelements is therefore elevated with a boost in viscosity ratio whereas deceleration is generated in the spin of microelements with increment in density ratio (owing to the inhibiting effect of a greater mass per unit volume on microstructural motions). It is noted from **Figure *10*** **and Figure 20** for all three applied pressure gradients, the dust particle velocity climbs significantly and fluid phase velocity also ascends slightly in Zone-II; however, the micro-polar fluid (linear) velocity is not displaced whereas the microrotation component (angular velocity) is weakly elevated in Zone-I with an increase in the ratio r_3.

5.Conclusions:

The unsteady flow of two immiscible Saffman dusty and Eringen micropolar fluids through a horizontal channel with both a stable and unstable interface has been analysed numerically, using a novel modified cubic B-spine differential quadrature method (MCB-DQM) with distinct computational schemes for the different zones. Extensive details of the discretization procedures in the MCB-DQM algorithm have been provided. The effects of the emerging hydrodynamic control procedures, for both regions, have been elaborated and four steps are necessary for the interface tracking computation. The impact of key hydrodynamic parameters i. e. Reynolds number, Froude number, particle concentration parameter, Eringen micropolar material parameter, volume fraction parameter, pressure gradient, time, viscosity ratio, and density ratio on fluid and particle velocities, microrotation (angular velocity component), and interface evolution have been computed and visualized graphically. The stability and fast convergence of the MCB-DQM algorithm have been confirmed. The core findings of the present analysis can be summarized in the following points:

-Under the horizontal channel scheme flow, *accelerating, oscillating and decelerating behavior* in the fluids and particle velocities, and micro-rotation profile with time are observed in respective Zones depending on whether the hydrodynamics is triggered by constant, periodic, or decaying pressure gradients, respectively.

-As anticipated, magnitudes of the fluid and particles velocities and micro-rotation components are enhanced with an increment in the pressure gradient.

-Increasing Reynolds number produces a marked enhancement in fluids and particle velocities, and micro-rotation profile for all cases of the applied constant, periodic, and decaying pressure gradient.

-Increasing the micropolar parameter affects the dust particle velocity and fluid velocity in the upper Zone even though the micropolar fluid is restricted to the Lower Zone. Hence increment in the parameter, flow leads to a diminution in both fluid and particle linear velocities, and also micro-rotation magnitudes (i.e., deceleration in the angular spin of the micro-elements in the micropolar fluid) with applied constant, periodic, or decaying pressure gradient.

-Elevation in dusty particle concentration parameter, increase the velocities of dust particle significantly for all three applied pressure gradient cases. This parameter is of course associated with Saffman dusty fluid which is present only in upper Zone fluid; however as noted in the discussion, the coupling of the dusty fluid momentum balance to the angular momentum balance of the micropolar liquid results in a delicate interplay between linear and angular velocity fields. This affects the microrotation profile for the lower zone fluid - hence the upper zone Saffman fluid velocity and lower zone micro-rotation profiles both slightly increase when the particle concentration parameter is enhanced for constant and periodic pressure gradient cases and slightly decreases for the decaying pressure case.

-A significant decline in dust particle and fluid velocities in the dusty fluid Zone (upper) is observed whereas there is no significant change in micropolar fluid velocity (lower zone) noted with an increase in the ratio of viscosity and density for all three applied pressure gradients. Micro-rotation increases significantly with an increment in the ratio of viscosities but considerably decreases with elevation in the ratio of densities.

The current study has demonstrated the excellent accuracy and stability characteristics of the modified cubic B-spine differential quadrature method (MCB-DQM) in numerical simulations of interfacial two-fluid (dusty-micropolar) duct flows. However, heat transfer and electromagnetic effects [54], [55] have been neglected. These may be considered in future studies and are also of relevance in biomedical and materials processing systems. Efforts in these directions will be communicated soon.

REFERENCES

[1] P. G. Saffman, “On the stability of laminar flow of a dusty gas,” *J. Fluid Mech.*, 1962, doi: 10.1017/S0022112062000555.

[2] D. H. Michael and D. A. Miller, “Plane parallel flow of a dusty gas,” *Mathematika*, 1966, doi: 10.1112/S0025579300004289.

[3] P. Mitra and P. Bhattacharyya, “Unsteady hydromagnetic laminar flow of a conducting dusty fluid between two parallel plates started impulsively from rest,” *Acta Mech.*, 1981, doi: 10.1007/BF01170340.

[4] P. Mitra and P. Bhattacharyya, Flow of a dusty gas between two parallel plates one stationary and other oscillating.,” *Def. Sci. J.*, 1981, doi: 10.14429/dsj.31.6359.

[5] P. Mitra and P. Bhattacharyya, “On the Hydromagnetic Flow of a Dusty Fluid Between Two Parallel Plates, One Being Stationary and the Other Oscillating,” *J. Phys. Soc. Japan*, 1981, doi: 10.1143/JPSJ.50.995.

[6] A. J. Chamkha, “Solutions for fluid-particle flow and heat transfer in a porous channel,” *Int. J. Eng. Sci.*, 1996, doi: 10.1016/0020-7225(96)00036-5.

[7] H. A. Attia, W. Abbas, M. A. M. Abdeen, and M. S. Emam, “Effect of porosity on the flow of a dusty fluid

between parallel plates with heat transfer and uniform suction and injection," *Eur. J. Environ. Civ. Eng.*, 2014, doi: 10.1080/19648189.2013.860923.

[8] H. A. Attia, W. Abbas, and M. A. M. Abdeen, "Ion slip effect on unsteady Couette flow of a dusty fluid in the presence of uniform suction and injection with heat transfer," *J. Brazilian Soc. Mech. Sci. Eng.*, 2016, doi: 10.1007/s40430-015-0311-y.

[9] H. A. Attia, "Unsteady MHD flow and heat transfer of dusty fluid between parallel plates with variable physical properties," *Appl. Math. Model.*, 2002, doi: 10.1016/S0307-904X(02)00049-5.

[10] H. A. Attia and K. M. Ewis, "Magnetohydrodynamic flow of continuous dusty particles and non-Newtonian Darcy fluids between parallel plates," *Adv. Mech. Eng.*, 2019, doi: 10.1177/1687814019857349.

[11] V. Singh and G. Singh, "Unsteady magnetohydrodynamic flow of a dusty fluid between two oscillating plates under varying constant pressure gradient," *Novi Sad J. Math.*, 2011.

[12] A. C. Eringen, "Mechanics of Micromorphic Continua," in *Mechanics of Generalized Continua*, 1968.

[13] A. Kucaba-Pietal, "Microchannels flow modelling with the micropolar fluid theory," *Bull. Polish Acad. Sci. Tech. Sci.*, 2004.

[14] O. A. Beg, H. S. Takhar, R. Bhargava, S. Sharma, and T. K. Hung, "Mathematical modeling of biomagnetic flow in a micropolar fluid-saturated darcian porous medium," *Int. J. Fluid Mech. Res.*, 2007, doi: 10.1615/InterJFluidMechRes.v34.i5.20.

[15] J. Peddieson, "An application of the micropolar fluid model to the calculation of a turbulent shear flow," *Int. J. Eng. Sci.*, 1972, doi: 10.1016/0020-7225(72)90072-9.

[16] S. Apparao, N. B. Naduviiiamani, and M. D. Patil, "Lubrication characteristics of porous inclined stepped composite bearings with couple stress fluids," *Tribol. Online*, 2013, doi: 10.2474/trol.8.234.

[17] C. Kang and A. Eringen, "The effect of microstructure on the rheological properties of blood," *Bull. Math. Biol.*, 1976, doi: 10.1016/s0092-8240(76)80030-4.

[18] M. Devakar and T. K. V. Iyengar, "Unsteady flows of a micropolar fluid between parallel plates using state space approach," *Eur. Phys. J. Plus*, 2013, doi: 10.1140/epjp/i2013-13041-1.

[19] S. Jangili and O. Anwar Bég, "Homotopy study of entropy generation in magnetized micropolar flow in a vertical parallel plate channel with buoyancy effect," *Heat Transf. Res.*, 2018, doi: 10.1615/HeatTransRes.2018018305.

[20] L. Wang, X. Chu, J. Wan, and C. Xiu, "Implementation of micropolar fluids model and hydrodynamic behavior analysis using user-defined function in FLUENT," *Adv. Mech. Eng.*, 2020, doi: 10.1177/1687814020943052.

[21] L. Wang, Y. Jian, and F. Li, "The flow of micropolar fluids through a microparallel corrugated channel," *Eur. Phys. J. Plus*, 2016, doi: 10.1140/epjp/i2016-16338-5.

[22] Y. Menni, A. Azzi, A. J. Chamkha, and S. Harmand, "Analysis of fluid dynamics and heat transfer in a rectangular duct with staggered baffles," *J. Appl. Comput. Mech.*, 2019, doi: 10.22055/JACM.2018.26023.1305.

[23] O. Anwar Beg *et al.*, "Computation of Non-isothermal thermo-convective micropolar fluid dynamics in a Hall mhd generator system with non-linear distending wall," *Int. J. Appl. Comput. Math.*, 2020, doi: 10.1007/s40819-020-0792-y.

[24] M. D. Shamshuddin, S. R. Sheri, and O. A. Bég, "Oscillatory dissipative conjugate heat and mass transfer in chemically reacting micropolar flow with wall couple stress: A finite element numerical study," *Proc. Inst. Mech. Eng. Part E J. Process Mech. Eng.*, 2019, doi: 10.1177/0954408917743372.

[25] O. A. Bég *et al.*, "Unsteady nonlinear magnetohydrodynamic micropolar transport phenomena with Hall and Ion-slip current effects: Numerical study," *Int. J. Appl. Electromagn. Mech.*, 2021, doi: 10.3233/JAE-201508.

[26] H. H. Sherief, M. S. Faltas, and K. E. Ragab, “Motion of a slip spherical particle near a planar micropolar-viscous interface,” *Eur. J. Mech. B/Fluids*, 2021, doi: 10.1016/j.euromechflu.2021.06.004.

[27] R. B. Bird, “Transport phenomena,” *Applied Mechanics Reviews*. 2002, doi: 10.1115/1.1424298.

[28] J. C. Umavathi, A. J. Chamkha, M. H. Manjula, and A. Al-Mudhaf, “Flow and heat transfer of a couple-stress fluid sandwiched between viscous fluid layers,” *Can. J. Phys.*, 2005, doi: 10.1139/p05-032.

[29] J. C. Umavathl, J. Prathap Kumar, and A. J. Chamkha, “Flow and heat transfer of a micropolar fluid sandwiched between viscous fluid layers,” *Can. J. Phys.*, 2008, doi: 10.1139/P08-022.

[30] A. K. Singh, A. K. Singh, and N. P. Singh, “Generalised couette flow of two immiscible viscous fluids with heat transfer using Brinkman model,” *Heat Mass Transf. und Stoffuebertragung*, 2004, doi: 10.1007/s00231-003-0421-4.

[31] A. K. Singh, “Convective flow of two immiscible viscous fluids using Brinkman model,” *Indian J. Pure Appl. Phys.*, 2005.

[32] J. C. Umavathi, J. Prathap Kumar, and A. J. Chamkha, “Convective flow of two immiscible viscous and couple stress permeable fluids through a vertical channel,” *Turkish J. Eng. Environ. Sci.*, 2009, doi: 10.3906/muh-0905-29.

[33] J. P. Kumar, J. C. Umavathi, A. J. Chamkha, and I. Pop, “Fully-developed free-convective flow of micropolar and viscous fluids in a vertical channel,” *Appl. Math. Model.*, 2010, doi: 10.1016/j.apm.2009.08.007.

[34] J. Srinivas and J. V. R. Murthy, “Flow of two immiscible couple stress fluids between two permeable beds,” *J. Appl. Fluid Mech.*, 2016, doi: 10.18869/acadpub.jafm.68.224.24013.

[35] J. Srinivas, J. V. Ramana Murthy, and K. S. Sai, “Entropy generation analysis of the flow of twoimmiscible couple stress fluids between two porous beds,” *Comput. Therm. Sci.*, 2015, doi: 10.1615/ComputThermalScien.2015012175.

[36] U. Rana, “Effect of dust particles on rotating micropolar fluid heated from below saturating a porous medium,” *Appl Appl Math*, 2009.

[37] A. Borrelli, G. Giantesio, and M. C. Patria, “Reverse flow in magnetoconvection of two immiscible fluids in a vertical channel,” *J. Fluids Eng. Trans. ASME*, 2017, doi: 10.1115/1.4036670.

[38] J. Srinivas, J. V. R. Murthy, and O. A. Bég, “Entropy generation analysis of radiative heat transfer effects on channel flow of two immiscible couple stress fluids,” *J. Brazilian Soc. Mech. Sci. Eng.*, 2017, doi: 10.1007/s40430-017-0752-6.

[39] R. K. Chandrawat, V. Joshi, O. Anwar Bég, and D. Tripathi, “Computation of unsteady generalized Couette flow and heat transfer in immiscible dusty and non-dusty fluids with viscous heating and wall suction effects using a modified cubic B-spine differential quadrature method,” *Heat Transf.*, 2021, doi: 10.1002/htj.22299.

[40] G. Tryggvason *et al.*, “A Front-Tracking Method for the Computations of Multiphase Flow,” *J. Comput. Phys.*, 2001, doi: 10.1006/jcph.2001.6726.

[41] A. Riaz and H. A. Tchelepi, “Numerical simulation of immiscible two-phase flow in porous media,” *Phys. Fluids*, 2006, doi: 10.1063/1.2166388.

[42] K. Vajravelu, P. V. Arunachalam, and S. Sreenadh, “Unsteady Flow of Two Immiscible Conducting Fluids Between Two Permeable Beds,” *J. Math. Anal. Appl.*, 1995, doi: 10.1006/jmaa.1995.1463.

[43] J. C. Umavathi, A. J. Chamkha, A. Mateen, and A. Al-Mudhaf, “Unsteady two-fluid flow and heat transfer in a horizontal channel,” *Heat Mass Transf. und Stoffuebertragung*, 2005, doi: 10.1007/s00231-004-0565-x.

[44] J. C. Umavathi, I. C. Liu, and M. Shekar, “Unsteady mixed convective heat transfer of two immiscible fluids confined between long vertical wavy wall and parallel flat wall,” *Appl. Math. Mech. (English Ed.*, 2012, doi:

10.1007/s10483-012-1596-6.

[45] M. Devakar, A. Raje, and S. Kumar, “Numerical Study on an Unsteady Flow of an Immiscible Micropolar Fluid Sandwiched Between Newtonian Fluids Through a Channel,” *J. Appl. Mech. Tech. Phys.*, 2018, doi: 10.1134/S0021894418060032.

[46] R. Bellman, B. G. Kashef, and J. Casti, “Differential quadrature: A technique for the rapid solution of nonlinear partial differential equations,” *J. Comput. Phys.*, 1972, doi: 10.1016/0021-9991(72)90089-7.

[47] J. R. Quan and C. T. Chang, “New insights in solving distributed system equations by the quadrature method-II. Numerical experiments,” *Comput. Chem. Eng.*, 1989, doi: 10.1016/0098-1354(89)87043-7.

[48] J. R. Quan and C. T. Chang, “New insights in solving distributed system equations by the quadrature method-I. Analysis,” *Comput. Chem. Eng.*, 1989, doi: 10.1016/0098-1354(89)85051-3.

[49] K. Ramesh and V. Joshi, “Numerical Solutions for Unsteady Flows of a Magnetohydrodynamic Jeffrey Fluid Between Parallel Plates Through a Porous Medium,” *Int. J. Comput. Methods Eng. Sci. Mech.*, 2019, doi: 10.1080/15502287.2018.1520322.

[50] R. Katta, R. K. Chandrawat, and V. Joshi, “A Numerical study of the unsteady flow of two immiscible micro polar and Newtonian fluids through a horizontal channel using DQM with B-Spline basis function,” *J. Phys. Conf. Ser.*, vol. 1531, no. 1, 2020, doi: 10.1088/1742-6596/1531/1/012090.

[51] R. K. Chandrawat, V. Joshi, and S. Kanchan, “Numerical simulation of interface tracking between two immiscible micropolar and dusty fluids,” *Mater. Today Proc.*, 2021, doi: 10.1016/j.matpr.2021.08.069.

[52] R. K. Chandrawat, V. Joshi, and O. Anwar Bég, “Ion Slip and Hall Effects on Generalized Time-Dependent Hydromagnetic Couette Flow of Immiscible Micropolar and Dusty Micropolar Fluids with Heat Transfer and Dissipation: A Numerical Study,” *J. Nanofluids*, vol. 10, no. 03, 2021, doi: 10.1166/jon.2021.1792.

[53] J. Zueco, P. Eguía, E. Granada, J. L. Míguez, and O. A. Bég, “An electrical network for the numerical solution of transient mhd couette flow of a dusty fluid: Effects of variable properties and hall current,” *Int. Commun. Heat Mass Transf.*, 2010, doi: 10.1016/j.icheatmasstransfer.2010.07.025.

[54] O. A. Bég, M. M. Rashidi, N. Rahimzadeh, T. A. Bég, and T. K. Hung, “Homotopy simulation of two-phase thermo-hemodynamic filtration in a high permeability blood purification device,” *J. Mech. Med. Biol.*, 2013, doi: 10.1142/S0219519413500668.

[55] O. A. Beg et al., , “Keller Box and Smoothed Particle Hydrodynamic Numerical Simulation of Two-Phase Transport in Blood Purification Auto-Transfusion Dialysis Hybrid Device with Stokes and Darcy Number Effects,” *J. Adv. Biotechnol. Bioeng.*, 2013, doi: 10.12970/2311-1755.2013.01.02.4.

[56] M. M. Bhatti, A. Zeeshan, N. Ijaz, O. Anwar Bég, and A. Kadir, “Mathematical modelling of nonlinear thermal radiation effects on EMHD peristaltic pumping of viscoelastic dusty fluid through a porous medium duct,” *Eng. Sci. Technol. an Int. J.*, 2017, doi: 10.1016/j.jestch.2016.11.003.

[57] M. Devakar and A. Raje, “A study on the unsteady flow of two immiscible micropolar and Newtonian fluids through a horizontal channel: A numerical approach,” *Eur. Phys. J. Plus*, 2018, doi: 10.1140/epjp/i2018-12011-5.

[58] M. Devakar and A. Raje, “A magnetohydrodynamic time dependent model of immiscible newtonian and micropolar fluids through a porous channel: A numerical approach,” *J. Appl. Fluid Mech.*, 2019, doi: 10.29252/jafm.12.02.28548.

[59] R. Niefer and P. N. Kaloni, “On the motion of a micropolar fluid drop in a viscous fluid,” *J. Eng. Math.*, 1980, doi: 10.1007/BF00037621.

[60] M. S. Faltas and E. I. Saad, “Slow motion of spherical droplet in a micropolar fluid flow perpendicular to a planar solid surface,” *Eur. J. Mech. B/Fluids*, 2014, doi: 10.1016/j.euromechflu.2014.04.010.